Electronic Structure of AlAs/GaAs and CdTe/HgTe Superlattices and Interfaces

Thesis by

Joel Nathan Schulman

In Partial Fulfillment of the Requirements

for the Degree of

Doctor of Philosophy

California Institute of Technology

Pasadena, California

1979

(Submitted May 22, 1979)

To

Leonard H. Schulman

and

Dinah B. Schulman

ACKNOWLEDGEMENTS

I would like to thank Professors Thomas McGill and Darryl Smith for their guidance and advice given frequently during my graduate career. I have also profited much from discussions with fellow graduate students Gordon Osbourn, John Best, Steve Lyon, Ken Elliott, Martin Chen, Peter Taborek, Anne Hofmeister and Ralph James. I am grateful for the financial support provided by Caltech and by fellowships from the International Business Machines Corporation and from the Metropolitan Life Insurance Company. I also very much appreciate Vere Snell for her help in many ways.

ABSTRACT

This thesis is concerned with reporting the results of a theoretical study of two semiconductor superlattices constructed parallel to (001) zincblende planes. One consists of alternating slabs of AlAs and GaAs, and the other of CdTe and HgTe. A tightbinding band structure calculation was done in order to find the energy levels and wave functions of these systems. Two aspects of the superlattice band structure were of particular interest - first, the nature and value of the band gap as a function of the thicknesses of the superlattice slabs and, second, the electronic structure of the interfaces between the constituent materials. These features were analyzed by referencing the superlattice results to relevant features of the constituent bulk band structures of AlAs, GaAs, CdTe, and HgTe. Through this procedure novel superlattice and interface quantum effects were identified and studied.

AlAs/GaAs Superlattice

The AlAs/GaAs superlattice is discussed first. The superlattice is found to have a semiconducting band gap for all ranges of AlAs and GaAs repeated slab thicknesses. The values of the gap are found to vary widely as the slab thicknesses are changed. For large slabs the gaps approach a value characteristic of bulk GaAs. They differ substantially from those of the random $Al_xGa_{1-x}As$ random alloy with the

same aluminum concentrations. The calculated band gaps are compared with the available experimental data and good agreement is found.

Whether the band gap is direct (conduction band minimum and valence band maximum occurring at the same point in $\vec{k}$ space) or indirect is determined. Again, behavior differing from the random alloy is noted. We find that certain superlattices can have direct band gaps with aluminum concentrations such that the corresponding random alloy would be indirect. This occurs due to the concentration of GaAs in slabs in the superlattice case. This effect is studied in detail for several ratios of AlAs to GaAs slab thicknesses.

The electronic states at the valence band maximum and the conduction band minimum are found to be affected greatly by the periodic superlattice potential. The AlAs slabs act as potential barriers to electrons and holes in the GaAs slabs at the band edges. The states therefore resemble the lowest energy states of a particle in a finite well. States with characteristic single and double peaked structures, like well states, are reported.

The AlAs/GaAs interface is investigated in the limit in which the superlattice slabs become large. Interface states are found near the boundaries of the Brillouin zone, but not at energies in the fundamental gap. The interface state density is too small to be observable as a separate peak in the calculated energy density of states. A layer density of states calculation shows that the superlattice is substantially bulk-like except for the layers directly adjacent to the interface.

CdTe/HgTe Superlattice

The CdTe/HgTe superlattice is reported on next. It is also found to be semiconducting. The values of the superlattice band gap decrease monotonically with increasing HgTe slab thickness for superlattices with specified cadmium concentrations. The band gaps of superlattices with the thinnest alternating slabs are close to the random $Hg_{1-x}Cd_xTe$ values. The gaps approach the zero band gap value of HgTe as the HgTe slab thickness increases. The material is always direct, in contrast with the AlAs/GaAs superlattice.

The symmetry of the state at the valence band maximum undergoes a transition as the HgTe slab thickness is increased. This is explained in terms of unusual features of the band structure of bulk HgTe. Well-like confinement of the conduction band minimum state, to a lesser degree than that found in the AlAs/GaAs superlattice, occurs in the HgTe slabs of the CdTe/HgTe superlattice. No hole confinement exists at the valence band maximum, unlike in the AlAs/GaAs case. These features are related to the band discontinuities between the two semiconductors making up the superlattice and their band structures.

The CdTe/HgTe interface is also investigated. Interface states are found, again near the Brillouin zone boundaries. In this case there is a state whose energy is the highest valence band energy at that point in $\vec{k}$ space, but it is still below the $\vec{k}$=0 valence band maximum energy.

Parts of this thesis have been or will be published under the following titles:

1. Band Structure of AlAs-GaAs (100) Superlattices, J. N. Schulman and T. C. McGill, Physical Review Letters 39, 1680 (1977).
2. Tight-binding Calculation for the AlAs-GaAs (100) Interface, J. N. Schulman and T. C. McGill, Journal of Vacuum Science and Technology 15, 1456 (1978).
3. The CdTe/HgTe Superlattice: Proposal for a New Infrared Material, J. N. Schulman and T. C. McGill, Applied Physics Letters, May 15, 1979.
4. Electronic Properties of the AlAs-GaAs (001) Interface and Superlattice, J. N. Schulman and T. C. McGill, Physical Review B, to be published.
5. Ideal CdTe/HgTe Superlattices, J. N. Schulman and T. C. McGill, submitted to the Journal of Vacuum Science and Technology.

TABLE OF CONTENTS

Chapter 1

INTRODUCTION

I. BACKGROUND

Recent advances in the technology of materials have led to the fabrication of new types of semiconductor based substances. Some of the most interesting of these are semiconductors with structures having very small characteristic sizes. One example with widespread technological importance is the integrated circuit on a silicon chip. The two-dimensional pattern on the surface of the chip can have features as small as a quarter of a micron. Another example, which can have even smaller characteristic lengths, is an epitaxially grown semiconductor. This consists of layers of semiconductors of varying composition and/or doping grown over a substrate material. Depending on the method of growth used, the layers can have thicknesses as small as several angstroms.

To study the properties of these materials consisting of small scale structures, we have carried out a theoretical investigation of two such systems - the AlAs/GaAs and the CdTe/HgTe superlattices. By superlattice is meant a material grown from alternating epitaxial slabs of the two constituent bulk substances. Our study of these superlattices with varying slab thicknesses explores several aspects of the electronic and optical properties of these new materials.

In the analysis of the electronic and optical properties of the materials, two factors become increasingly important as the size of the structures decrease. First, the interfaces which form the boundaries

between the different regions of the material play a more substantial role in determining the properties. The commonly used approximation of a crystalline solid as an unbounded material extending to infinity in all directions applies only to uniform, macroscopic systems. For these small scale structures an effort must also be made to understand the nature of the electronic states of the previously ignored boundaries and how they match up with the bulk electronic character of the solid. Many of the bulk properties of solids have been successfully explained within the framework of band theory. Bulk band theory must be modified when considering these interface features. The two most serious modifications which must be dealt with are the lack of crystal periodicity in the direction perpendicular to the interface and the unknown positions of the atoms at the interface. These problems will be discussed later.

The second factor which becomes important is that the small sizes of the structures induce new quantum mechanical phenomena. Again, approximations made when considering macroscopic systems are no longer valid. For example, the electronic behavior of semiconductor heterojunctions (junctions made from two different semiconductors) is usually considered to be explainable in terms of the bulk band structures of the two component materials on either side of the junction away from the interface. If the junctions are repeated by alternating the two semiconductors and forming a superlattice, this approximation will still be valid for thick enough alternating slabs. As the thickness

is decreased, it will no longer be valid to use the bulk band structures in analyzing the properties of the essentially new material.

The AlAs/GaAs and CdTe/HgTe systems were chosen for theoretical investigation because of their apparent simplicity. All four semiconductors crystallize in the zincblende lattice structure with two atoms per unit cell at normal temperatures and pressures. The constituents of each pair have the same lattice spacings to a high degree. In both cases there is a difference in lattice constants of less than .3 percent[1,2]. The calculation is also made less complicated by the fact there are common anions, arsenic in one case and tellurium in the other. The differing cations in each system are the smallest possible perturbation from a homogeneous solid because the cations are directly adjacent to each other in the same column of the periodic table of the elements. Thus they have similar chemical character and almost identical ion size. The lattice constant match-up is evidence for the mildness of this perturbation. In our calculation we ignore the small lattice discontinuity and assume a perfect lattice match at the interface. This is probably a good approximation since the small strain between the two lattice constants most likely results in a single, average lattice constant for the superlattice.

An additional reason for studying the AlAs/GaAs superlattice is that this system has actually been made in the laboratory[3,4]. The molecular beam epitaxy technique (MBE) is capable of producing layered structures on an atomically fine scale. Samples with repeated superlattice slabs consisting of just two atomic monolayers (one each of

AlAs and GaAs) made using MBE have been reported on in the literature[5]. The method of construction involves the carefully timed shuttering of three elemental sources, each at its appropriate temperature. The molecular beams from the sources are aimed at a substrate on top of which the crystal is grown. Growth is parallel to (001) zincblende planes, which are polar, i.e., terminate in layers consisting of all anions or all cations. The superlattice structures thus made were checked by several methods, including transmission electron microscopy, x-ray diffraction, optical measurements, and Raman analysis of the phonon spectra. The interfaces were found to be not perfectly abrupt. Approximately twenty-five percent of the cation sites were disordered at the interface between the AlAs and GaAs layers[6]. Due to the small Al-Ga interdiffusion constant at growth temperatures, this disorder extends only about 5 Å away from the interface in both directions [7].

The CdTe/HgTe superlattice has not yet been fabricated. The high vapor pressure of mercury creates a different set of problems from those associated with the AlAs/GaAs superlattice[8]. Efforts are presently being made by some laboratories to adapt the MBE technique to solve these problems. It is likely that in the near future the CdTe/HgTe superlattice will be made, either by using MBE or by using some other technique. The only other superlattice that has been successfully grown to date is that made from the III-V compounds InAs and GaSb.

There have been a number of experiments done on the AlAs/GaAs

superlattice which will be related to our calculation. Of primary importance are optical measurements [5,9]. These experiments can determine the energy level separations between occupied and unoccupied electronic states. The results of our band structure calculation can then be directly compared with the experimental values. Optical absorption, luminescence, and reflectivity, analyzed as a function of outgoing photon energy, all have been used. In particular, the energies of the semiconducting band gaps have been determined in this way.

Another important experiment for our purposes has been the determination of the phonon spectra of the superlattice using Raman scattering [6,10]. In this technique the phonon energy corresponds to the energy lost by a scattered photon. Although we have not calculated any phonon energies, this experiment is relevant for the following reason. It has been used to study the abruptness of the AlAs/GaAs interface by comparing experimental spectra with theoretical spectra calculated assuming different degrees of interfacial disorder. It thus helps to evaluate the expected accuracy of our calculation, which assumes perfectly abrupt interfaces, when compared with the aforementioned optical measurements of band energies. This will be discussed further in Chapter 3.

To investigate the two-dimensional nature of some of the electronic states of the superlattice, another experimental technique has been used. This involved looking for the Shubnikov-de Haas oscillations associated with quantum sub-bands produced by the superlattice periodicity superimposed on the bulk zincblende structure [11]. These

oscillations in the resistance of the material as a function of applied magnetic field give information about the shape of the slice of the Fermi surface perpendicular to the field. Applying the field in various directions relative to the direction of periodicity explores the asymmetry of the superlattice. These results can be compared qualitatively with the results of our band structure calculations, although this has not yet been done.

Previous to our calculation, most of these experiments have been analyzed using a simple theoretical model - the well model. The wells referred to come about because of the difference in band gaps of the two constituent materials, AlAs and GaAs. The large band gap of AlAs (2.25 eV) overlaps the smaller band gap of GaAs (1.5 eV). The band gap difference is split up between a valence band discontinuity and a conduction band discontinuity. These discontinuities form the sides of the wells for electrons and holes in the GaAs slabs. The superlattice is envisioned as consisting of these alternating GaAs wells and AlAs barriers. The electrons and holes near the band extrema were regarded as free particles confined in the wells, but with their characteristic effective masses. The magnitudes of the discontinuities were determined by adjusting them to reproduce some feature of the experimental results [9,12,13]. This model obviously applies only to features of the band structure near the band gap. It is also necessary for each repeated slab to consist of several atomic layers in order

for the effective mass approximation to be applicable. To investigate more of the band structure or to consider superlattices with atomically thin repeated slabs, a more detailed calculation which includes the atomic potentials must be used.

There have been two such detailed calculational methods used on the superlattice system - the pseudopotential method and the tight-binding method. In this thesis we use the empirical tight-binding method to study the band structure of the AlAs/GaAs and CdTe/HgTe (001) superlattices. The tight-binding method has the advantage of being comparatively easy to use. It is also very flexible in that superlattices with different slab thicknesses can be dealt with simply by changing a single parameter in the calculation. Quantities of interest can thus be calculated as a function of thickness and trends noted. The many parameters in a tight-binding calculation are in a sense an advantage in that they already contain much information about the bulk constituents of the superlattice. The tight-binding method has also been used to study the InAs/GaSb superlattice [14].

The pseudopotential method, as has been applied to the superlattice system, is also an empirical method in that it uses parameters that are related to either atomic quantities or bulk band structure quantities as inputs to the calculation. It is more complex and costly than a tight-binding calculation, but it is supposedly closer to a first principles approach because it has fewer adjustable parameters. Despite this, the two pseudopotential calculations done on the AlAs/GaAs

(001) superlattice [15,16] disagree with each other, as will be discussed in Chapter 3. The other pseudopotential calculation was done on the AlAs/GaAs (110) superlattice [14].

II. Outline of Thesis

The subsequent sections of this thesis are divided into three parts. The first part, Chapter 2, describes the tight-binding method and how it is applied to calculate the band structure of superlattices. The formalism of tight-binding is described and the approximations inherent in the method are set forth.

Chapter 3 discusses the results of our calculation for the AlAs/GaAs superlattice. The nature and value of the semiconducting band gap of several sets of superlattices are determined, in particular whether they are direct or indirect. The influence of the thickness of the AlAs and GaAs repeated slabs is studied. The effect of the periodic potential of the superlattice on the states at the band extrema and the relationship of these states to bulk GaAs states is noted. For superlattices with the thickest slabs, the existence of interface states is investigated. The abruptness of the interface is determined and layers near the interface compared with the bulk electronic character.

The CdTe/HgTe superlattice is the subject of Chapter 4. Features similar to those of the AlAs/GaAs superlattice are investigated. The unusual band structure of HgTe, the band discontinuities between CdTe and HgTe, and the importance of the spin-orbit interaction make the electronic character of this superlattice distinctive. The band gap as a function of slab thickness is studied and compared with that of the random alloy with the same composition. A cross-

over in symmetry character of the valence band maximum as slab thickness is varied is found and explained in terms of the bulk band structures of HgTe and CdTe. Interface states are also investigated for this superlattice.

III. SUMMARY OF MAIN RESULTS

AlAs/GaAs Superlattice and Interface

1. The band gaps of the superlattice as a function of AlAs and GaAs slab thicknesses are determined. The gaps differ substantially from those of the $Al_xGa_{1-x}As$ random alloys with the same composition. The direct or indirect nature of the lowest energy gap is determined and explained.

2. The natures of the electronic states at the conduction band minimum and the valence band maximum are found. The discontinuities in the conduction and valence band edges between the two bulk materials cause these states to be localized in the GaAs slabs.

3. Interface states are identified in the superlattice consisting of ten layers of GaAs and ten of AlAs. They appear in the superlattice band structure as new energy levels appearing where there were gaps in the bulk band structures of the individual constituents. Examination of the electronic states at these energies show them to be localized within a few atomic layers of the interface. No interface states are found with energies in the semiconducting band gap.

4. A layer density of states calculation reveals that the electronic character of the interface is abrupt. Only the layer densities of states for layers directly adjacent to the interface differ substantially from the bulk densities of states of the individual constituents.

CdTe/HgTe Superlattice and Interface

1. The band gaps of these superlattices are found to decrease monotonically with increasing HgTe slab thickness for fixed ratios of CdTe to HgTe slab thicknesses. The band gaps of thin slabbed superlattices are close to those of the random $Hg_{1-x}Cd_xTe$ alloy of the same composition.

2. The symmetry of the valence band maximum state is found to change at certain HgTe slab thicknesses. This is explained by relating the superlattice states to bulk CdTe and HgTe states and by using group theory.

3. The existence of interface states is investigated for the superlattice with twelve layers of CdTe alternating with twelve of HgTe. Interface states are found near the boundaries of the Brillouin zone, but not in the semiconducting band gap.

4. The confinement of the states at the conduction band minimum and valence band maximum are investigated and related to the bulk band structures. The valence band maximum state is found to be delocalized. the conduction band minimum state is localized, but less so than for the AlAs/GaAs superlattice.

References to Chapter 1

1. A. G. Milnes and D. L. Feucht, Heterojunctions and Metal-Semiconductor Junctions (Academic Press, New York, 1972).
2. R. Dornhaus and G. Nimtz, Springer Tracts in Modern Physics 78 (1976).
3. L. L. Chang, L. Esaki, W. E. Howard, R. Ludeke, and G. Schul, J. Vac. Sci. Technol. 10, 655 (1973).
4. R. Dingle, A. C. Gossard, and W. Wiegmann, Phys. Rev. Lett. 34, 1327 (1975).
5. A. C. Gossard, P. M. Petroff, W. Weigmann, R. Dingle, and A. Savage, Appl. Phys. Lett. 29, 323 (1976).
6. J. L. Merz, A. S. Barker, Jr., and A. C. Gossard, Appl. Phys. Lett. 31, 117 (1977).
7. Raymond Dingle, Proceedings of the Thirteenth International Conference on the Physics of Semiconductors, Rome, pp 965-974, (1976).
8. Private communication from L. L. Chang.
9. R. Tsu, A. Koma, and L. Esaki, J. of Appl. Phys. 46, 842 (1975).
10. P. Manuel, G. A. Sai-Halasz, L. L. Chang, Chin-An Chang, and L. Esaki, Phys. Rev. Lett. 37, 1701 (1976).
11. L. L. Chang, H. Sakaki, C. A. Chang, and L. Esaki, Phys. Rev. Lett. 38, 1489 (1977).
12. R. Dingle, W. Wiegmann, and C. H. Henry, Phys. Rev. Lett. 33, 827 (1974).

13. D. Mukherji and B. R. Nag, Phys. Rev. B12, 4338 (1975).

14. R. N. Nucho and A. Madhukar, J. Vac. Sci. Technol. 15, 1530 (1978).

15. E. Caruthers and P. J. Lin-Chung, J. Vac. Sci. Technol. 15, 1459 (1978).

16. W. Andreoni, A. Baldereschi, and R. Car, Solid State Commun. 27, 821 (1978).

17. W. E. Pickett and M. L. Cohen, J. Vac. Sci. Technol. 15, 1437 (1978).

Chapter 2

SUPERLATTICE BAND STRUCTURE CALCULATION

I. Outline of Procedure

The tight-binding method used here to calculate superlattice electronic properties consists of several steps. First, the bulk band structures of the two constituent materials are obtained. This is done by constructing a bulk Hamiltonian matrix using a limited basis set. Each matrix element consists of overlap integrals with the Hamiltonian between wavefunctions centered on the same ion and ions separated by specified distances and directions. No integrals are actually evaluated. Instead, the integrals are parameterized and the parameters determined by duplicating certain features of the known bulk band structures. The number of parameters depends on the symmetry of the crystal lattice, the size of the basis set used, and the number of neighboring ions included.

The second step is to construct a Hamiltonian matrix for the superlattice. The parameters determined to fit the bulk band structures are used here. This procedure thus includes much bulk information via these parameters. The size of the resulting matrix is determined by the chosen thicknesses of the repeated slabs.

There is one additional parameter which must be determined and inserted into the superlattice matrix - the relative band lineups between the two bulk band structures. When the bulk band structures were fit in the first step, the zero of energy was set arbitrarily. The tight-binding procedure as used here does not give the absolute energies or energies relative to the vacuum level. The superlattice matrix includes the parameters for the two materials and therefore

requires knowledge of this offset parameter. Its value must be found from sources external to the tight-binding calculation itself. The procedures used to do this will be described in detail. Once this parameter is determined, certain diagonal matrix elements of the superlattice matrix are adjusted appropriately.

The next step is to diagonalize the superlattice Hamiltonian matrix. The resulting eigenvalues and eigenvectors are the electron energies and the coefficients of the basis orbitals of the wave functions at those energies. The superlattice band structure comes about from diagonalizing the matrix for different values of the electron momentum vector $\vec{k}$. The symmetry of a particular electron state can be found from examining the symmetry of the basis orbital coefficients.

This procedure has several advantages over the well model. It takes into account the atomic potentials out of which the wells are made, although it still uses the band discontinuities deduced from experiment using the well model in the thick slab limit. A more complete band structure is produced including all the valence bands. Detailed results about the electronic states are easily obtained. Also, the spin-orbit interaction can be taken into account using the tight-binding method, unlike the well model. In the following section the tight-binding method and formalism will be described in detail.

II. Tight-binding Method

II.1 Bulk Crystal

Our tight-binding approach is closely related to that first presented in detail by Slater and Koster [1]. The calculation is done within the single particle framework. That is, the effects of all the other electrons on a given electron are summarized by a one body potential.

Since the total Hamiltonian of this system is periodic, it can be diagonalized into blocks characterized by values of $\vec{k}$, the electron momentum operator in the periodic crystal. The eigenvectors of each of the Hamiltonian sub-matrices take the Bloch form and are thus eigenvectors of the crystal translation operator as well as energy eigenvectors. This does not have to be the case. Instead, the energy eigenvectors could have been chosen to be eigenvectors of the crystal point group. The operations of translation and the point group operations both commute with the Hamiltonian. Unfortunately, they do not, in general, commute with each other and thus cannot be simultaneously diagonalized. It is most convenient in the tight-binding method to diagonalize the translation operations. At special points in $\vec{k}$ space of high symmetry, however, some operations of the point group can be applied and the electron wave functions labeled by the particular representation of the group to which they belong. This is a useful procedure in relating superlattice state to bulk states, as will be shown.

Bloch's theorem states that the wave functions in a periodic

crystal will be made from linear combinations of functions which take the form

$$u_i(\vec{k},\vec{r}) = \frac{1}{\sqrt{N}} \sum_{\vec{T}} e^{i\vec{k}\cdot\vec{T}} \phi_i(\vec{r}-\vec{T}-\vec{\tau}_i) \qquad (2.1)$$

The sum is over $\vec{T}$, the positions of all unit cells in the crystal. The vector $\vec{\tau}_i$ is the position of the atom in the unit cell about which the orbital ϕ_i is centered. As there may be several orbitals centered about each atom, $\vec{\tau}_i$ may be the same vector for several values of the subscript i. The normalizing factor preceding the summation involves N, the number of unit cells in a large region which is repeated with periodic boundary conditions.

The orbitals ϕ_i resemble the wave functions of electrons around atoms in that they are centered about atomic nuclei. The u_i, therefore, are sums of these atomic-like orbitals, one per unit cell, modulated by the exponential phase factor. The actual electron wave function is a linear combination of the u_i with coefficients c_i to be determined -

$$\psi(\vec{k},\vec{r}) = \sum_i c_i(\vec{k})\, u_i(\vec{k},\vec{r}) \quad . \qquad (2.2)$$

So far there have been no approximations in this single particle picture. The first approximation of the tight-binding method is to limit the number of orbitals, ϕ_i, in the sum in Eq. (2.1). The energy bands of concern are produced by the overlapping of wave functions which are not too different from isolated atomic wave functions. Only a few localized, atomic-like orbitals are needed to describe these

bands. This is especially true for the valence bands, but even the qualitative behavior of the lower energy conduction bands can be accounted for with a small number of orbitals [2]. The orbitals used in our calculation will be described in Chapters 3 and 4.

The coefficients c_i in Eq. (2.2) are found by finding stationary points in the energy

$$E = \langle\psi|H|\psi\rangle \tag{2.3}$$

with respect to the c_i. This is equivalent to finding the eigenvalues and eigenvectors of the matrix

$$H_{ij} = \langle u_i|H|u_j\rangle \quad . \tag{2.4}$$

Using the explicit form for u_i and u_j in Eq. (2.1) results in the equation

$$H_{ij} = \frac{1}{N} \sum_{T,T'} e^{i\vec{k}\cdot(\vec{T}-\vec{T}')} \int d^3\chi\phi_i^*(\vec{r}-\vec{T}-\vec{\tau}_i)H(\vec{r})\phi_j(\vec{r}-\vec{T}-\vec{\tau}_j) \quad . \tag{2.5}$$

The translational symmetry of the problem is manifested in the fact that the integral in Eq. (2.5) depends only on the vector difference between $\vec{T}$ and $\vec{T}'$, and not on their separate values. Thus $\vec{T}'$ can be set equal to zero and the summation over $\vec{T}'$ replaced by an additional factor of N. In addition, the integral can then be symbolized in an obvious way by $V_{ij}(\vec{T})$ resulting in the simplified equation

$$H_{ij} = \sum_{\vec{T}} e^{i\vec{k}\cdot\vec{T}} V_{ij}(\vec{T}) \quad . \tag{2.6}$$

At this stage the second major approximation in this method must be made. The sum in Eq. (2.6) extends over arbitrarily large values of $\vec{T}$. It gets progressively more difficult to evaluate more than a few of the integrals in this sum. For most systems of interest it has been found necessary to keep only a few terms. The sum is divided up into spherical shells of atoms centered on the $\vec{T}' = 0$ unit cell. The approximation is made to ignore the integrals involving atoms outside a certain shell radius. The integrals left out are not necessarily small, and there are an increasing number of them for a given shell as $|\vec{T}|$ increases. This would be a serious difficulty if these integrals were actually evaluated and used to calculate H_{ij}. It would result in errors substantially larger than those caused by the first approximation which limited the basis set [2].

Instead, these integrals are parameterized. Values of the V_{ij} are chosen such that the energies resulting from diagonalizing H_{ij} reproduce as closely as possible specific features of the bulk band structures. In particular, an attempt is made to duplicate the energies of known optical transitions which have been measured experimentally. If more exact band structure calculations are available, such as those using the pseudopotential method, they can also be used to supply energy values to be fit.

The integrals that are chosen to be parameterized contain in an average way, through the fitting procedure, information left out in

ignoring the other integrals. The tight-binding method in the empirical form used here is seen to be a method of interpolation, filling in the band structure between points in $\vec{k}$ space with known energy. The tight-binding Hamiltonian incorporates the crystal symmetry and approximates the wave function nature through the limited basis set. This guarantees that the bands will qualitatively resemble the true band structure. The fitted energies tie down the bands to their known values at certain points. The following chapters give the results of this procedure for the four bulk zincblende semiconductors involved in this study.

A simple example of how a matrix element of H_{ij} is actually obtained using the V_{ij} parameters will now be given. Consider the matrix element between orbitals ϕ_0 and ϕ_1, both of S-type symmetry, centered on adjacent anions and cations, respectively, in the zincblende lattice. By S-type symmetry is meant that the orbitals behave like the lowest order spherical harmonic under the operations of the point group. They do not have to be invariant under the full rotation group, however. Each anion has four nearest neighbor cations located at the positions

$$\vec{\tau} = \frac{a}{4}(1,1,1),\ \frac{a}{4}(1,-1,-1),\ \frac{a}{4}(-1,1,-1),\frac{a}{4}(-1,-1,1) \quad . \qquad (2.7)$$

The distance a is the length of the side of the conventional zincblende unit cell. The symmetry of the crystal ensures that V_{01} is the same

number for all four vectors $\vec{\tau}$. In similar ways for the other integrals, symmetry greatly reduces the number of independent V_{ij}. The sum in Eq. (2.6) for the nearest neighbors only is then

$$H_{ol} = V_{ol}(e^{i\frac{a}{4}(k_x+k_y+k_z)} + e^{i\frac{a}{4}(k_x-k_y-k_z)}$$

$$+ e^{i\frac{a}{4}(-k_x+k_y-k_z)} + e^{i\frac{a}{4}(-k_x-k_y+k_z)}) \qquad (2.8)$$

$$= 4V_{ol}(\cos\frac{k_x a}{4}\cos\frac{k_y a}{4}\cos\frac{k_z a}{4} - i\sin\frac{k_x a}{4}\sin\frac{k_y a}{4}\sin\frac{k_z a}{4}) \quad .$$

Including more shells of atoms would add terms to this sum with additional V_{ij} parameters. It would not increase the size of the matrix, which is determined purely by the number of basis orbitals per unit cell.

II.2 Superlattice

The tight-binding method as applied to the superlattice is no different in principle from that used in the bulk case. The major difference is that the unit cell is enlarged over the bulk zincblende unit cell by a factor depending on the repeat distance of the superlattice slabs. Consider the superlattice shown in Fig. 2.1. It shows a cross section of a (001) superlattice made from alternating slabs of two materials. Each slab consists of two layers of one of the materials (a single (001) layer consists of an infinite plane of all anions and an infinite plane of all cations). Let the repeat distance perpendicular to the interface be called ℓ. For a superlattice with M layers of one material and N layers of the other,

$$\ell = (M + N) \times a/2 \tag{2.9}$$

where a is the length of the side of the conventional zincblende unit cell. Instead of the two atoms per unit cell of the zincblende crystal, there are now 2x(M+N) atoms per unit cell of length ℓ. The number of orbitals per unit cell and thus the size of the Hamiltonian matrix are multiplied by this same factor of M+N as compared with the bulk.

The parameters obtained in fitting the bulk band structures are used in the matrix elements of the superlattice Hamiltonian. The matrix elements are of two kinds. The first kind are matrix elements between orbitals centered on the same material, i.e., within each slab. There are also matrix between orbitals centered on atoms in adjacent slabs,

Figure 2.1

Cross-section of a superlattice consisting of two atomic layers of one material alternating with two atomic layers of another. The length of the superlattice unit cell in the direction perpendicular to the interfaces is ℓ.

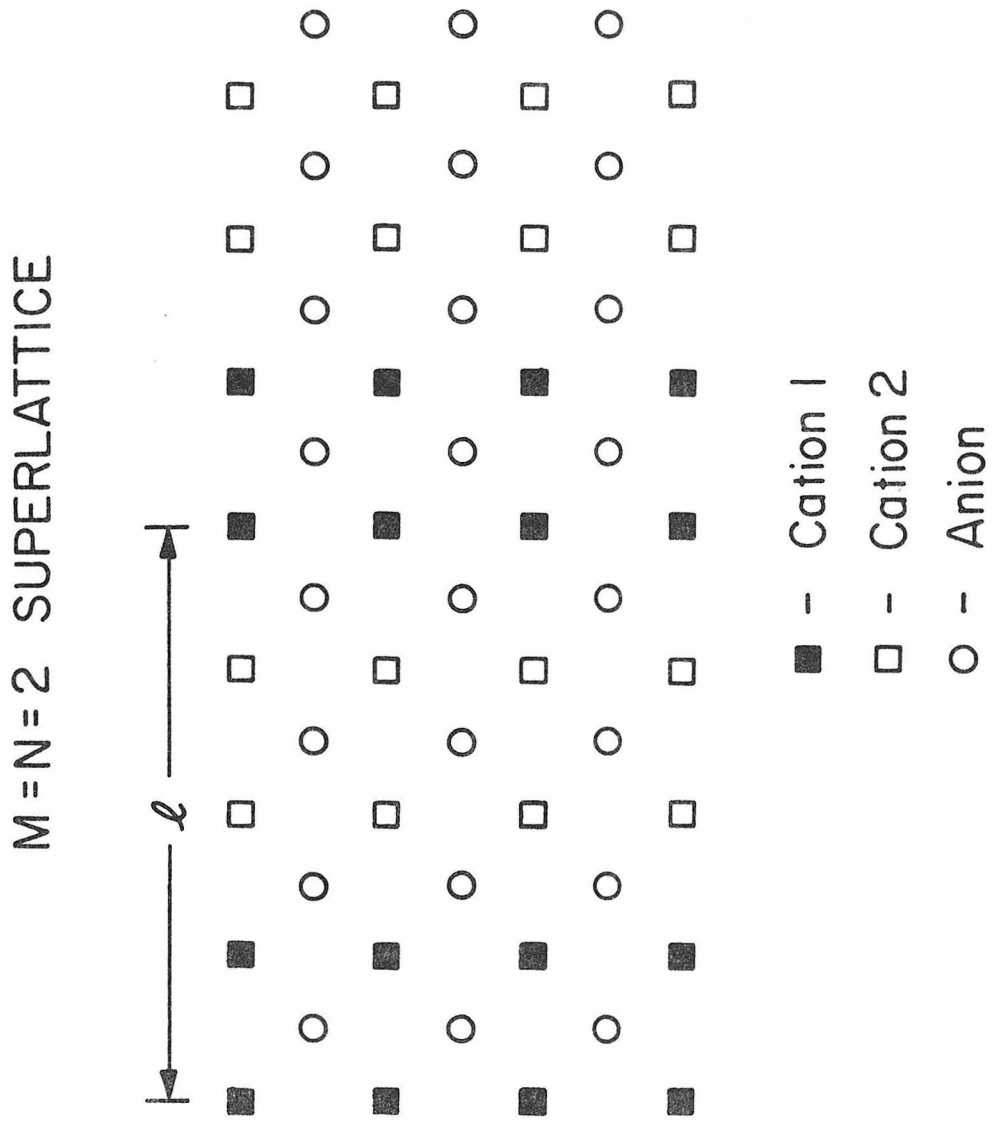

Figure 2.1

i.e., between aluminum atoms and gallium atoms in the AlAs/GaAs superlattice. The bulk parameters do not supply values for the matrix elements of the second kind. Instead, an averaging procedure is used, as described in Chapter 3.

The band structure of a given superlattice is easily obtained. The eigenvalues resulting from diagonalizing the Hamiltonian matrix are the electronic band energies for one point in $\vec{k}$ space. Repeating the diagonalization procedure for different values of $\vec{k}$ produces a band structure. The number of bands is fixed by the number of basis orbitals used per unit cell. Thus there are M+N times as many superlattice bands as bulk bands. There is, however, a compensating decrease in the size of the Brillouin zone by the same factor. This is because the size of the Brillouin zone in reciprocal space is inversely proportional to the unit cell size in real space. The net result is that there is the same number of states per unit cell in reciprocal space in both cases.

The eigenvectors of the Hamiltonian are useful in obtaining information about the electronic states of the superlattice. The information is only partial, however. Since actual orbitals are not used in the calculation, the precise spatial distribution of the wave functions cannot be determined. All that are available are the coefficients of each orbital in the total wave function. There are two types of information available from the orbital coefficients. First, the symmetry of the state can be identified. This is done by examining the relative signs of the coefficients and comparing with the predictions of

group theory. The usefulness of this information will be seen in the subsequent chapters. Second, the values of the coefficients give an estimate of the spatial distribution of the wave function. The approximation can be made that the orbitals are substantially localized on a given atom only and that their amplitudes on neighboring atoms are ignorable. A charge density per atom can then be calculated for that wave function. This information can then also be used to calculate layer densities of states and valence charge densities as will be shown.

More details of the bulk and superlattice tight-binding calculations will be given as they are needed in Chapters 3 and 4.

References to Chapter 2

1. J. C. Slater and G. F. Koster, Phys. Rev. 94, 1498 (1954).

2. D. J. Chadi, Phys. Rev. B16, 3572 (1977).

Chapter 3

AlAs/GaAs SUPERLATTICE AND INTERFACE

I. Introduction

As reviewed in the last chapter, the AlAs/GaAs superlattice is an especially interesting system to study because it has been fabricated in recent years using molecular beam epitaxy [1,2]. This superlattice is in effect a new man-made material. Since the superlattices consist of a series of interfaces between AlAs and GaAs, they offer an opportunity to investigate the properties of these interfaces as well as the superlattice itself.

This system is suitable for a theoretical study of superlattices since the structure may closely approximate an ideal model. The two materials have the same crystal structure and they have lattice constants which differ by about 0.1%. The lattice constant of AlAs is 5.661 $\mathring{A}$, and that of GaAs is 5.654 $\mathring{A}$ [3]. Hence, the structures tend to form with a minimum amount of defecting at the interface. The similar chemical nature of the Ga and Al atoms makes it likely that there is not a large amount of relaxation of the atoms at the interface. The small interdiffusion coefficients reported for Ga and Al in this system [4,5] and Raman scattering studies of the phonon spectrum [6] suggest that the interface is rather abrupt. For these reasons we approximate this system by a series of abrupt interfaces between AlAs and GaAs. This approximation may break down for the thinnest superlattice slabs, as will be discussed.

As the ability to fabricate and analyze MBE grown materials has improved, attempts have been made to measure their more complex prop-

erties. Superlattice effects on electron and phonon energy levels have been extensively investigated. Most experiments were analyzed using a simple theory. AlAs, having an indirect band gap of 2.25 eV at $0^{o}K$, is envisioned as forming a series of barriers to electrons and holes in the GaAs, which has a smaller direct gap (Fig. 3.1). The conduction and valence band discontinuities (ΔE_c and ΔE_v), which form the sides of the barriers, must be determined. Dingle, Wiegmann, and Henry [7] measured the splitting in the optical absorption spectra of two peaks due to transitions from electrons in the lowest GaAs conduction band well state to the light and to the heavy hole states in the GaAs valence band well. They fit this splitting using a valence band discontinuity equal to 15% of the energy gap difference between GaAs and $Al_xGa_{1-x}As$. The samples they used had x values less than .3, resulting in direct $Al_xGa_{1-x}As$. We consider slabs consisting of pure AlAs, whose smallest gap is indirect. In determining the discontinuities in our case, we assumed that the 15% gap difference applied to the difference in the direct gaps of the two materials. There have been efforts to predict the band discontinuities in this and other systems a priori using more detailed pseudopotential methods[8]. So far these methods have not been successful for AlAs/GaAs.

The electrons and holes in the well models were assumed to have effective masses which were related to their bulk GaAs values. Mukherji and Nag [9] used a somewhat more complicated model which took into account the non-parabolicity of the bands and also the relevant band structure of the $Al_xGa_{1-x}As$ layers which made up the sides of the wells.

Figure 3.1

Well model of AlAs/GaAs superlattice. The smaller band gapped GaAs forms wells between AlAs barriers for the electrons and holes near the band edges. ΔE_V and ΔE_C are the valence and conduction band discontinuities between the AlAs and GaAs.

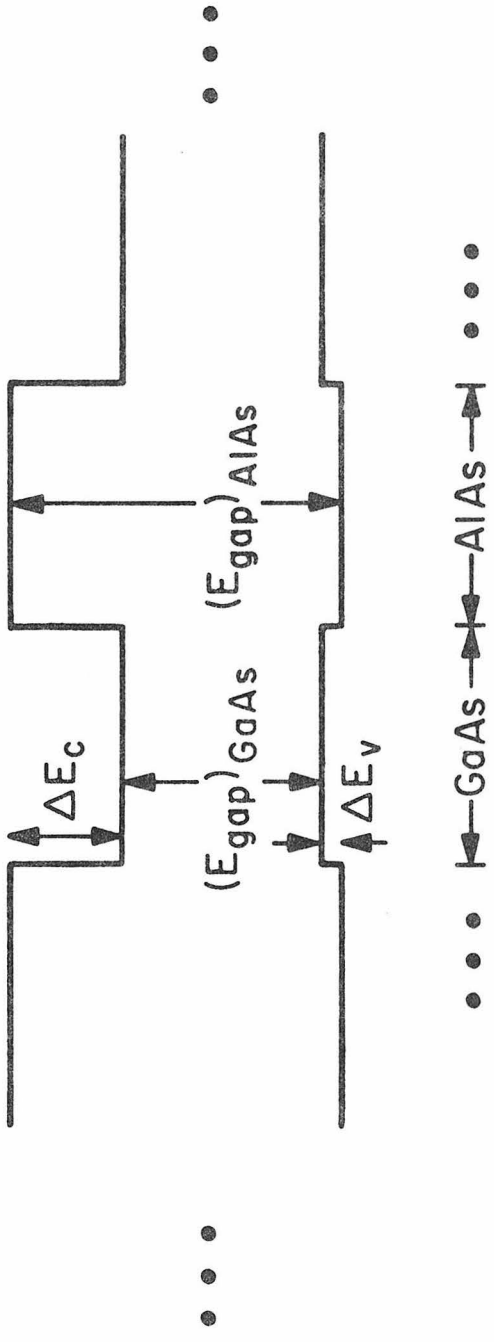

Figure 3.1

Recently two pseudopotential calculations have been done with somewhat conflicting results concerning the location and nature of the lowest conduction band in the alternating monolayer superlattice[10,11]. Section IV discusses these results.

We have done tight-binding calculations for superlattices with alternating slabs of various thicknesses. In the succeeding sections we will report the details of these calculations and the most important properties observed from them. Section II reviews the tight-binding method and how it applies to the semiconductor-semiconductor interface and superlattice. The procedure used to obtain matrix element parameters is also described. Section III describes results pertaining to the band gap behavior and character of the valence and conduction band states near the band gap edges as a function of slab thickness. The results of our calculation will be compared to those obtained by others as they pertain to the alternating monolayer superlattice in Section IV. A comparison of our results with available experimental data is given in Section V. The existence and location of interface states are discussed in Section VI. Finally, Section VII deals with the question of charge transfer and the close to bulk-like nature of layers near the interface as determined by the layer density of states.

II. Calculation

The basic method we have used is similar to that used in previous surface band structure calculations for diamond and zincblende structures. The important difference is that now there are two types of semiconductors forming the interface, replacing the semiconductor-vacuum interface. The two-dimensional periodicity parallel to the interface is preserved. The interface is repeated, therefore avoiding the problem of additional semiconductor-vacuum interfaces. This forms the semiconductor-semiconductor superlattice.

The tight-binding matrix elements of the superlattice matrix are taken over directly from bulk values. These values are determined separately for AlAs and GaAs by adjusting them to reproduce certain low temperature bulk energy levels. The valence band discontinuity equal to 15% of the direct gap difference is then subtracted from the four AlAs diagonal bulk parameters. The resulting parameters are listed in Table 1. The bulk energy values used were gotten from two pseudopotential calculations: one by Hess, et al. for AlAs [14], and a nonlocal calculation by Chelikowsky and Cohen for GaAs [15]. The pseudopotential and resulting tight-binding energies are listed in Table II.

A total of eight tight-binding wave functions per unit cell were used in the bulk calculation, giving an 8 by 8 matrix to be diagonalized

TABLE I. Tight-binding parameters for AlAs and GaAs determined by fitting to bulk pseudopotential calculations.[12] The notation is that of Ref. 13. The subscripts 0 and 1 designate anion and cation, respectively. All parameters are given in units of eV. The valence band discontinuity has been subtracted from the AlAs parameters.

		AlAs	GaAs
1.	$Ess(000)_0$	-6.343	-6.953
2.	$Ess(000)_1$	-1.467	-2.254
3.	$Exx(000)_0$	1.974	1.338
4.	$Exx(000)_1$	1.394	1.839
5.	$Ess(\frac{1}{2},\frac{1}{2},\frac{1}{2})$	-1.817	-1.774
6.	$Esx(\frac{1}{2},\frac{1}{2},\frac{1}{2})_{01}$	1.326	1.304
7.	$Esx(\frac{1}{2},\frac{1}{2},\frac{1}{2})_{10}$	1.001	1.121
8.	$Exx(\frac{1}{2},\frac{1}{2},\frac{1}{2})$	.515	.479
9.	$Exy(\frac{1}{2},\frac{1}{2},\frac{1}{2})$	1.237	1.447
10.	$Exy(110)_0$	.321	.295
11.	$Exy(110)_1$	.264	.195
12.	$Exx(110)_0$	.189	.200
13.	$Exx(110)_1$	.220	.207
14.	$Exx(011)_0$	- .492	- .347
15.	$Exx(011)_1$	- .218	- .282
16.	$Esx(110)_0$	.026	.001
17.	$Esx(110)_1$	.059	.018
18.	$Ess(110)_0$	- .007	- .002
19.	$Ess(110)_1$	- .144	- .178

TABLE II. Pseudopotential eigenvalues used in the parameter fitting procedure and tight-binding eigenvalues. Energies are in eV.

Level	AlAs		GaAs	
	Tight-binding	Ref. 14	Tight-binding	Ref. 15
Γ_1^v	-12.06	-11.66	-12.89	-12.55
Γ_{15}^v	0	0	0	0
Γ_1^c	2.82	3.21	1.53	1.51
Γ_{15}^c	4.19	4.57	3.91	4.55
X_1^v	-9.46	-9.42	-9.96	-9.83
X_3^v	-5.02	-5.55	-6.08	-6.88
X_5^v	-1.72	-1.97	-2.94	-2.99
X_1^c	2.30	2.25	2.07	2.03
X_3^c	3.01	2.62	2.88	2.38
L_1^v	-9.94	-10.07	-10.42	-10.60
L_2^v	-5.85	- 5.52	- 7.19	- 6.83
L_3^v	- .48	- .70	- 1.28	- 1.42
L_1^c	2.64	2.76	1.89	1.82
L_3^c	4.81	5.15	5.78	5.47

for the energy eigenvalues and eigenvectors. One s-type wave function and three p-type wave functions (P_x,P_y,P_z) were used for both the anion (As) and for the cation (Al,Ga). The eight wave functions produced four valence bands and four conduction bands, each band being doubly degenerate as the spin-orbit interaction was neglected. All possible nearest neighbor matrix element parameters were included. Symmetry considerations reduced the number of such parameters in zinc-blende materials to nine. The valence bands were fit well with just these parameters. To improve the conduction band fit, particularly the shapes of the bands, additional second nearest neighbor parameters were included. The use of d-orbitals would be necessary to improve the conduction bands further [16]. The resulting bulk band structures are shown in Fig. 3.2. Comparison of our bulk results with those of Ref. 14 and Ref. 15 show good agreement, even with the lower conduction bands. The tight-binding calculation is unable to produce as much curvature in the conduction bands as the pseudopotential calculations although the general shapes are accurate.

Once the bulk tight-binding parameters are determined, the tight-binding matrix for the superlattice using them can be formed. The matrix is organized in eight by eight blocks (Fig. 3.3) representing the integrals between tight-binding orbitals centered on the same and different atomic layers. Each layer contains a single anion and cation per unit cell with four orbitals each. Because only integrals up to

Figure 3.2

Bulk band structures of AlAs and GaAs using the tight-binding method.

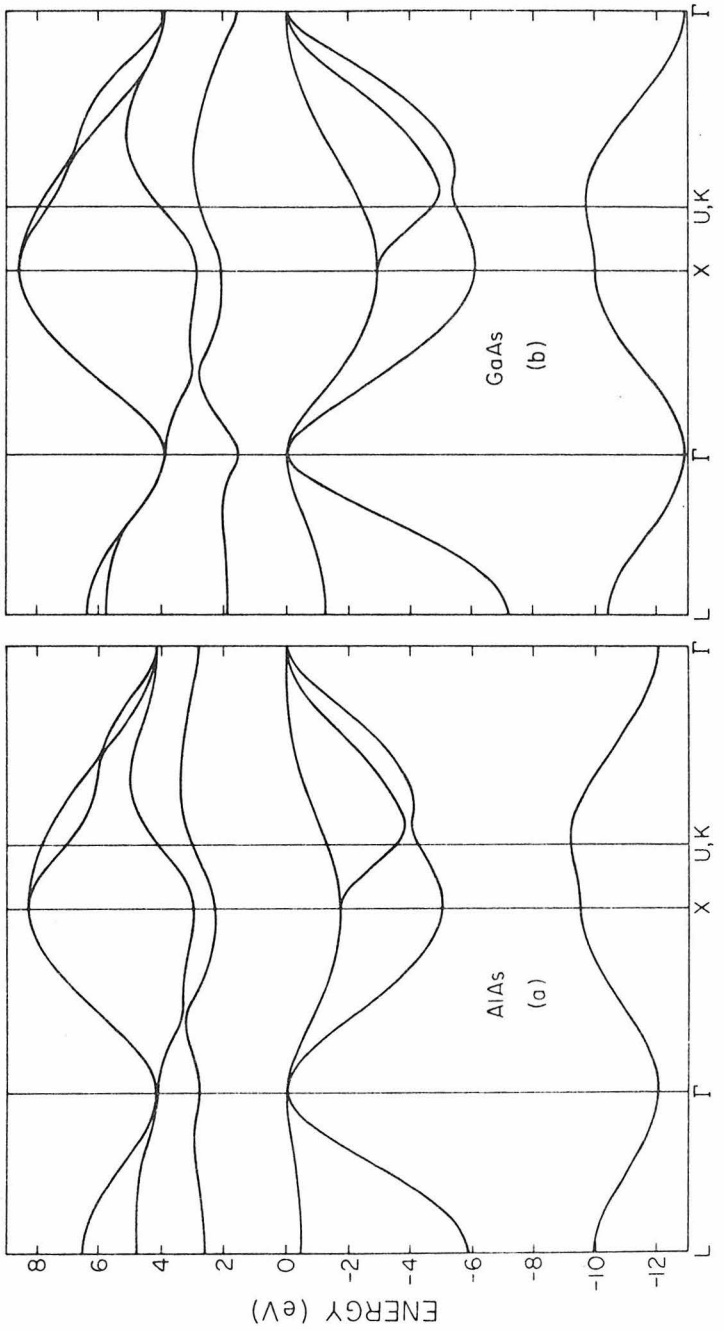

Figure 3.2

Figure 3.3

Superlattice tight-binding matrix. Each block represents an eight by eight sub-matrix. The upper righthand corner block, "β", links AlAs and GaAs slabs and has both of those types of parameters. The matrix is organized such that each block has matrix elements between orbitals centered on atoms in the same (A and a) or adjacent (B, b, or β) superlattice layers.

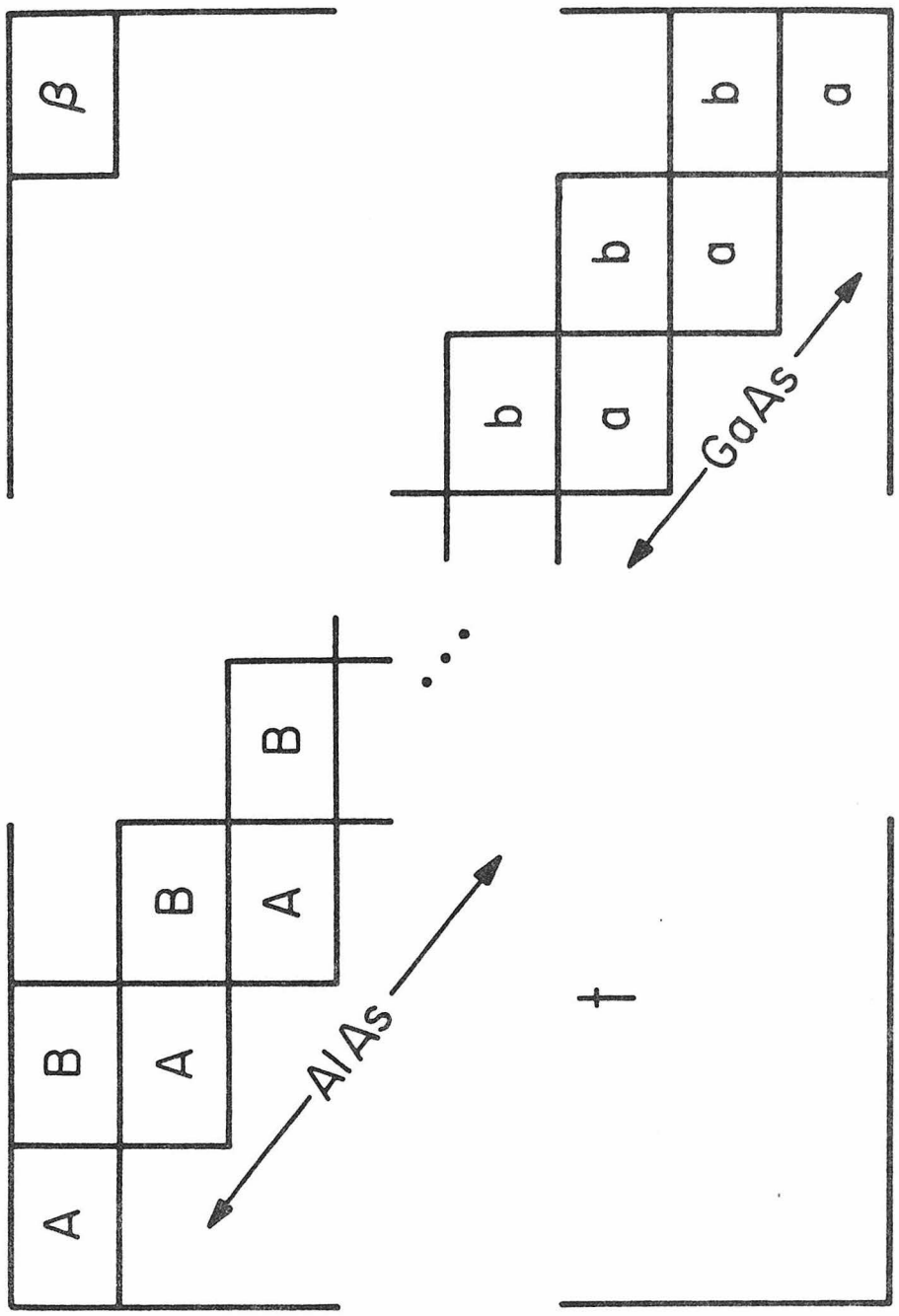

Figure 3.3

second nearest neighbors are used, there are just two types of eight by eight blocks. The blocks down the diagonal (labelled A and a) contain matrix elements between orbitals within a layer including the eight self-energy integrals between a given orbital and itself. The four AlAs self-energy parameters have the previously discussed valence band discontinuity value subtracted off from them. Matrix elements between adjacent layers (labelled B, b and β) are located in blocks that are just off-diagonal and in one extra block each at the upper right-hand corner and lower lefthand corner. The corner blocks contain the integrals between adjacent layers where each layer is in an adjacent slab. These blocks are the major difference between this matrix and the matrix used for surface calculations. With its matrix elements equal to zero, the surface tight-binding matrix results. It also incorporates an extra phase factor of $e^{ik_z d}$ where d is the slab width and k_z is the component of the k-vector perpendicular to the interface. Letting M equal the number of AlAs layers per slab and N the number of GaAs layers per slab, the total size of the superlattice matrix is $((M+N) \times 8)^2$.

The AlAs and GaAs share common As ions right at the interface. There is therefore no problem determining the matrix elements at the nearest neighbor level there. The bulk values were used. Second nearest neighbor matrix elements, however, connect Al and Ga centered orbitals. The bulk fitting procedure does not supply parameters in

this case. Instead, a simple average of Al to Al and Ga to Ga parameters was used. Also, the As to As second nearest neighbor parameters were somewhat different in the AlAs and the GaAs. Again an average was used. The lattice match of the interface was assumed to be perfect. No relaxation or reconstruction was assumed.

The eigenvalues and eigenvectors obtained from diagonalizing the tightbinding matrix can be used to calculate an approximate layer density of states for the superlattice. An exact layer density of states cannot be found due to the fact that the wave functions are unknown. Only the coefficients of the localized orbitals that make up the wave functions are available. Although these orbitals might have non-zero amplitudes on layers other than those on which they are centered, it is assumed that this spreading is small and is thus neglected. The layer density of states in a given energy interval and layer is calculated by summing the squares of the localized orbital coefficients centered on that layer for wave functions whose energies are within the energy interval. We used several thousand energies calculated at points in k-space throughout the Brillouin zone and binned with an energy resolution of .1 eV. An approximate layer valence charge density can also be calculated by summing up the layer density of states for all the valence band energies.

III. Band Gap Properties

Both bulk AlAs and bulk GaAs are semiconductors, having band gaps of 2.25 eV [14] (indirect) and 1.51 eV [15] (direct), respectively. When AlAs and GaAs are deposited alternately in a superlattice, the resulting structure has some properties which are intermediate between the two bulk materials and some completely new properties. In particular, the superlattice material is still found to be semiconducting, but it does not resemble the $Al_xGa_{1-x}As$ alloy of the same Al concentration. This is true even for very thin alternating slabs. Fig. 3.4 shows the behavior of the superlattice band gaps as a function of the number of atomic monolayers of GaAs (N) per repeated slab. The energy gaps at three points in k space are plotted: Γ, J, and K (see inset). The curve labelled Γ represents the direct gap. In the coordinate system whose axes are parallel to the edges of the conventional zincblende unit cell of side length a, J has the coordinates $\frac{2\pi}{a}$ (.5, .5, 0). The z-axis is taken to be perpendicular to the superlattice slabs. The J-point has what would correspond to the bulk zincblende L-point ($\frac{2\pi}{a}$ (.5, .5, .5)) folded into it when (M+N)/2 is even. For both AlAs and GaAs, there is a local minimum in the bottommost conduction band

Figure 3.4

Energy gaps from the top of the valence band to the lowest conduction band energies at Γ, J, and K. The location of these points in the slice of $\vec{k}$-space parallel to the interfaces is shown in the inset to (c). N is the number of atomic monolayers of GaAs per repeated slab. Three ratios of AlAs to GaAs slab thicknesses (M:N) are shown: (a) 1:2 (b) 1:1 (c) 2:1.

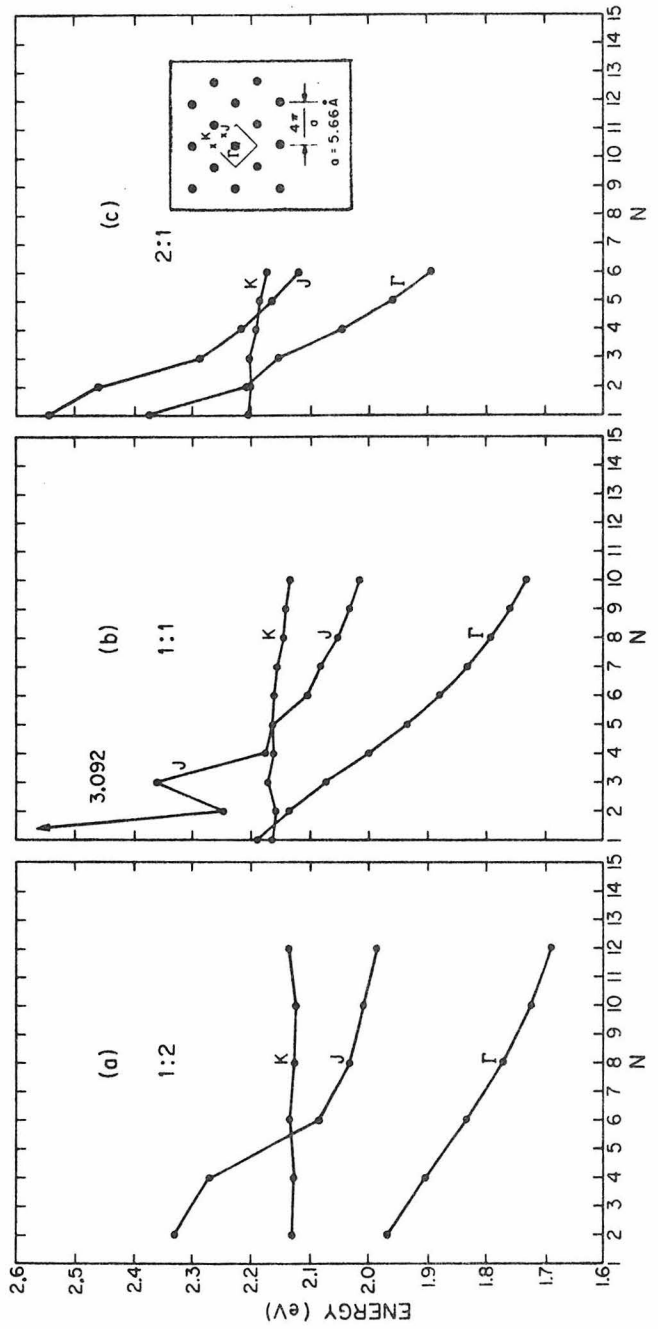

Figure 3.4

near the L-point. The J-point is also a local minimum in the superlattice case. The same is true of the K-point which has the zinc-blende X-point ($\frac{2\pi}{a}$ (1,0,0)) mapped onto it. The lowest of the curves in Fig. 3.4 for a given slab thickness determines whether the material is direct or indirect. The band gaps are all relative to the valence band maxima of the superlattices. Three cases are shown in Fig. 3.4 for three different ratios of AlAs to GaAs slab thicknesses: (a) 1:2, (b) 1:1, (c) 2:1. This corresponds to values of x for the $Al_xGa_{1-x}As$ alloy of 1/3, 1/2, and 2/3. As the number of GaAs monolayers per slab increases, the gap values approach their bulk GaAs values of 1.5 eV for Γ, 2.1 eV for X, and 1.9 eV for L. The values calculated for the thickest GaAs slab are shown in Fig. 3.4(a) for N=12. The Γ and J gaps (1.7 eV and 2.0 eV) are still not very close to their bulk values. The K-point gap, however, is seen to be uniformly flat for all N. This is because the bulk X-point conduction band energies of AlAs and GaAs relative to their valence band maxima are separated by an amount approximately equal to the valence band off-set (.19 eV) between the two materials. When this off-set is subtracted from the AlAs diagonal parameters, as previously described, the energies at the two bulk X-points are approximately the same. There is, therefore, no well confining the electrons to either the AlAs or GaAs slabs. This is confirmed by examining the state at this energy. In Fig. 3.5 is plotted

Figure 3.5

Anion (As) and cation (Al and Ga) charge distributions for the state at the conduction band minimum at K for the superlattice consisting of five layers of AlAs alternating with ten layers of GaAs. Separate curves for the anion and cation are given. The numbers on the horizontal axis label the cation (Al, Ga) positions.

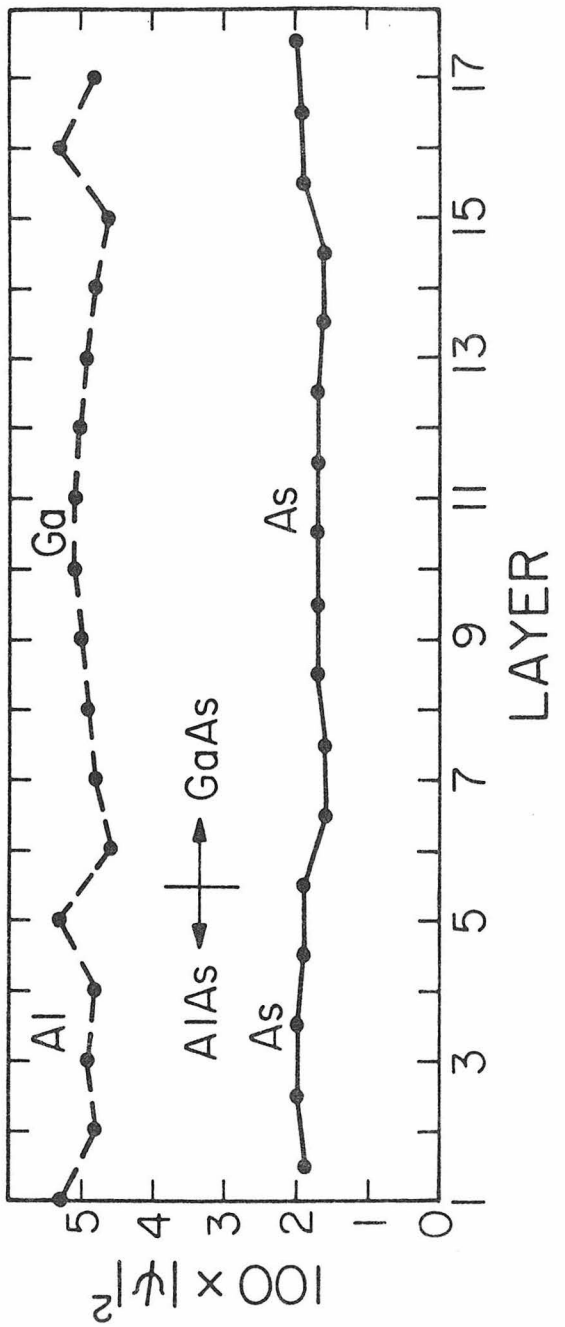

Figure 3.5

the total squared amplitude on the anion and cation at each layer for the case M=5, N=10. Layers labeled 1 through 5 are AlAs and layers 6 through 15 are GaAs. It is highly uniform in the direction perpendicular to the interface with close to the same amplitudes on AlAs and GaAs. Both the Γ and L-point conduction band energies, by contrast, are higher in AlAs. This tends to confine the electrons to the GaAs slabs. Thicker slabs mean wider wells and therefore lower ground state well energies.

A typical set of GaAs band gap edge well-like states at the Γ-point is shown in Fig. 3.6. In this case ten layers of AlAs alternate with ten layers of GaAs. Five different energies are shown in Fig. 3.6(a) through (e), in order of increasing energy. The states shown in Fig. 3.6 (b) and (c) with energies -.074 eV and -.052 eV form a triplet of states (including the double degeneracy of the -.052 eV state) originating from the triply degenerate zincblende Γ_{15} symmetry state. The disruption of periodicity in the z direction splits off one state leaving the states with x and y-type symmetry degenerate. These three states all have the characteristic single peaked shape of the lowest well potential eigenfunction. Figure 3.6(a) shows the double peaked structure characteristic of the next well potential eigenfunction. The next state lower in energy (not shown) is located mostly on the AlAs layers. The situation is similar for the conduction band states in Fig. 3.6(d) and (e). Both single and double peaked eigenfunctions are found. There are other well-like states with energies above these.

Figure 3.6

Charge distributions for five states with energies as shown at Γ for the superlattice consisting of ten layers of AlAs alternating with ten layers of GaAs.

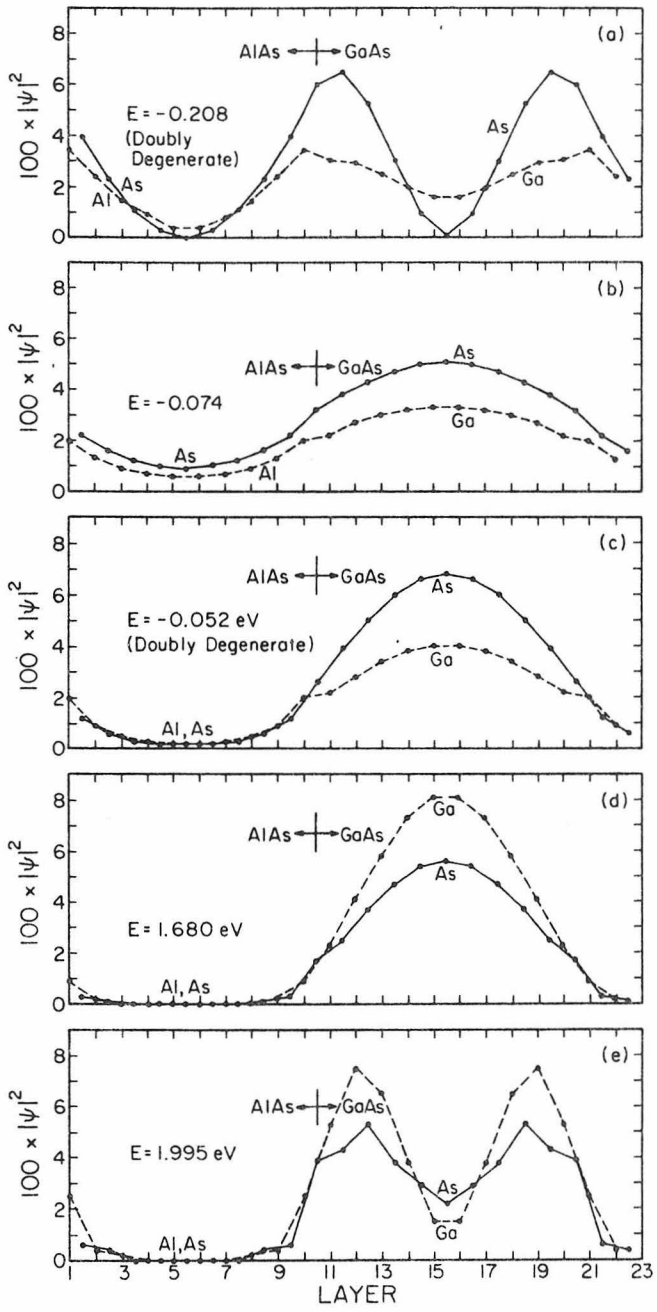
(a)
AlAs GaAs
E = -0.208
(Doubly
Degenerate)
Al
As
As
Ga
(b)
AlAs GaAs
E = -0.074
As
Al
As
Ga
(c)
AlAs GaAs
E = -0.052 eV
(Doubly Degenerate)
Al, As
As
Ga
(d)
AlAs GaAs
E = 1.680 eV
Al, As
Ga
As
(e)
AlAs GaAs
E = 1.995 eV
Al, As
As
Ga
100 × |ψ|²
LAYER
1 3 5 7 9 11 13 15 17 19 21 23
0 2 4 6 8

Figure 3.6

The electronic states formed when very thin slabs of AlAs and GaAs are alternated in a superlattice are more difficult to analyze. The energy gap at the K-point remains nearly constant in all three cases shown in Fig. 3.4 as previously explained. The J-point curve in Fig. 3.4(b) is no longer monotonic for small N. This is explained by examining in detail which bulk states are mapped onto the J-point. These are states with bulk $\vec{k}$ values of $\frac{2\pi}{a}(\frac{1}{2}, \frac{1}{2}, \frac{2n}{I})$, where I is the total number of layers of AlAs plus GaAs per slab (M+N) and n takes on the values 1 through I. Therefore it is only for even values of I/2 that the J-point includes the bulk L-point. It is exactly for these values of N that the J-point curve is lower. The gap values at N=1 and 3 are higher because they represent the energies of points in bulk k-space near but not at L. The energies at these bulk points are indeed higher than at the L-point. As N increases beyond three the J-point includes bulk values of $\vec{k}$ so close to L that their energies are indistinguishable from those at the L-point. Results obtained using a previous set of parameters [17] do not show this feature because of the flatness of the bulk conduction bands produced by them. The K-point contains bulk $\vec{k}$ values of $\frac{2\pi}{a}(1,0,\frac{2n}{I})$ and thus includes the X-point whenever n=0 for any I.

IV. Other Calculations

As mentioned in Section I, there have been two other calculations done on the alternating monolayer AlAs/GaAs superlattice [10,11]. This section compares the results of these calculations with ours concerning an important point of disagreement which exists about the value and nature of the lowest conduction band state of this superlattice. Our calculation and the pseudopotential calculation done by Andreoni, et al. [11] find that the alternating monolayer superlattice is similar to the random $Al_{.5}Ga_{.5}As$ alloy as regards to this state. Caruthers and Lin-Chung [10] in their pseudopotential calculation find a substantially smaller value of the band gap than that found in the random alloy.

Our results concerning the nature of this state for thin slabbed superlattices, including the monolayer superlattice,will first be discussed. The relevant feature of Fig. 3.4 is the direct-indirect transition determined by the relative energy gap values at Γ and K. The alloy $Al_xGa_{1-x}As$ has an indirect band gap at the X-point for values of x greater than about .35 [18]. The X-point is mapped onto the Γ-point for even values of I, as the bulk values associated with Γ are given by $\frac{2\pi}{a}(0,0,\frac{2n}{I})$. Thus there are X-points mapped onto both Γ and K. In Fig. 3.4(b) and (c) the K-point curve is seen to cross the Γ-point curve for small N, indicating that the X-point associated with the K-point has a smaller energy there. Examining the state at Γ for the case N=1 in Fig. 3.4(b) reveals that it is of Γ_4 symmetry which would be the case for an X_1 symmetry bulk state mapped onto the

Γ-point. The state symmetries for N greater than one are Γ_1 type confirming that they originate from bulk Γ_1 symmetry states. Caruthers and Lin-Chung [10] in their pseudopotential calculation find that the Γ_4 state has the lowest conduction band energy for M=N=1 by several tenths of eV's. This is a large departure from what would be expected from considering the bulk band structures or the $Al_{.5}Ga_{.5}As$ alloy. Our results are closer to the alloy energies, as calculated by simply averaging the AlAs and GaAs tight-binding parameters. The results of this calculation are shown in Table III.

Andreoni, et al., find that the band structure of the monolayer superlattice differs from that of the random alloy with the same composition by only tens of millivolts. They trace the discrepancy between their results and those of Caruthers and Lin-Chung to differing choices of cation potentials, and give theoretical evidence for the superiority of their choice. Although our calculation is in closer agreement with theirs than with Caruthers and Lin-Chung's, this matter has yet to be resolved with certainty. The experimental results for this superlattice are discussed in the next section.

TABLE III. Energy values at the bottom of the conduction band calculated using tight-binding parameters. Results are shown at the zinc-blende Γ, X, and L-points. The energy of the valence band maximum is zero in all cases. The point in $\vec{k}$-space appropriate to the superlattice is shown in parentheses. Energies are in eV. $a = 5.66\text{A}^{o}$

	$\underline{\Gamma}$	$\underline{X}$	$\underline{L}$
AlAs	2.83	2.30	2.64
GaAs	1.53	2.07	1.89
Alloy (x=.5)	2.18	2.18	2.27
M=N=1 Superlattice	2.19 $(\frac{2\pi}{a}(0,0,0))$	2.16 $(\frac{2\pi}{a}(1,0,0))$	2.17 $(\frac{2\pi}{a}(\frac{1}{2},\frac{1}{2},\frac{1}{2}))$

V. Comparison with Experiment

This section discusses the results of optical experiments done on the AlAs/GaAs superlattice and compares them with our calculation. R. Tsu, A. Koma, and L. Esaki [19] determined the band gap of a superlattice consisting of sixteen layers each of AlAs and GaAs using reflectivity measurements. They found a value of 1.63 eV. Unfortunately, this superlattice is slightly too large for our computing capacity to handle. The lowest curve in Fig. 3.4(b), if extended out to N=16, would certainly be consistent with this value.

Gossard, et al. [20] have measured the band gaps of three superlattices for which we have also made calculations. For a superlattice with one layer of AlAs alternating with eight of GaAs, they observed an exciton peak in the absorption spectrum at 1.675 eV. Our calculation does not include exciton effects. We calculate a direct band gap of 1.66 eV for this superlattice. The two values agree within the accuracy of the tight-binding method. They also show an optical emission spectrum for the superlattice with three layers of AlAs and six of GaAs. The peak of their emission spectrum occurs near 1.85 eV [21]. We calculate 1.83 eV for the band gap of this superlattice.

The third superlattice for which Gossard, et al., have measured the band gap is the alternating atomic monolayer superlattice. There is some discrepancy between the measured and calculated band gaps for this case. Their experiment determined that the optical absorption edge is near 2 eV. We calculate a value of 2.19 eV for this gap.

Agreement would not be expected to be as good for this atomically thin superlattice as for the others. This is because the presently unavoidable cation disorder in the MBE process makes this superlattice only about 25% more ordered than the random alloy [6]. Our calculation applies to ideally ordered systems and thus should not agree as well in this case.

VI. Interface States

The band structure in representative directions of the superlattice consisting of four layers of AlAs alternating with four layers of GaAs is shown in Fig. 3.7. The two directions perpendicular to the interface have less dispersion than the directions parallel to the interface. This is especially true near the valence band maxima and the conduction band minima. In both of the two perpendicular directions there is a slight rise in energy at the bottom of the conduction band toward the Brillouin zone edge. This feature is held in common with superlattices of other layer thicknesses. In this case the bottommost conduction band energy increases by 50 meV from $\frac{2\pi}{a}(0,0,0)$ to $\frac{2\pi}{a}(0,0,\frac{1}{8})$ and by 190 meV from $\frac{2\pi}{a}(1,0,0)$ to $\frac{2\pi}{a}(1,0,\frac{1}{8})$.

The superlattice band structure shown in Fig. 3.7 for this thin slabbed superlattice has no obvious split-off bands which might need to be identified with localized states. It can approximately be described as a combination of the AlAs and GaAs three-dimensional bulk bands mapped onto the two-dimensional superlattice reciprocal space. Instead of the eight energy bands (ignoring degeneracy) found in the bulk band structures, there are now 8x(M+N) bands reflecting the fact that there are M+N as many basis wave-functions in the enlarged superlattice unit cell.

For larger slab thicknesses, split-off bands characteristic of interface states start to appear. An interface state is here defined as a state having non-zero amplitudes on layers only within two or three layers of the interface. In Fig. 3.8 are shown the valence bands near the J-point for the superlattice with M=N=10. Only a small volume in reciprocal lattice space near the J-point is found to have definite interface states. The interface states at the J-point are states which are split off from high concentrations of bands. This is

Figure 3.7

Band structure of the AlAs/GaAs superlattice consisting of four monolayers of AlAs alternating with four monolayers of GaAs. The quantity a is the length of the side of the conventional zincblende unit cell. It equals 5.66 Å.

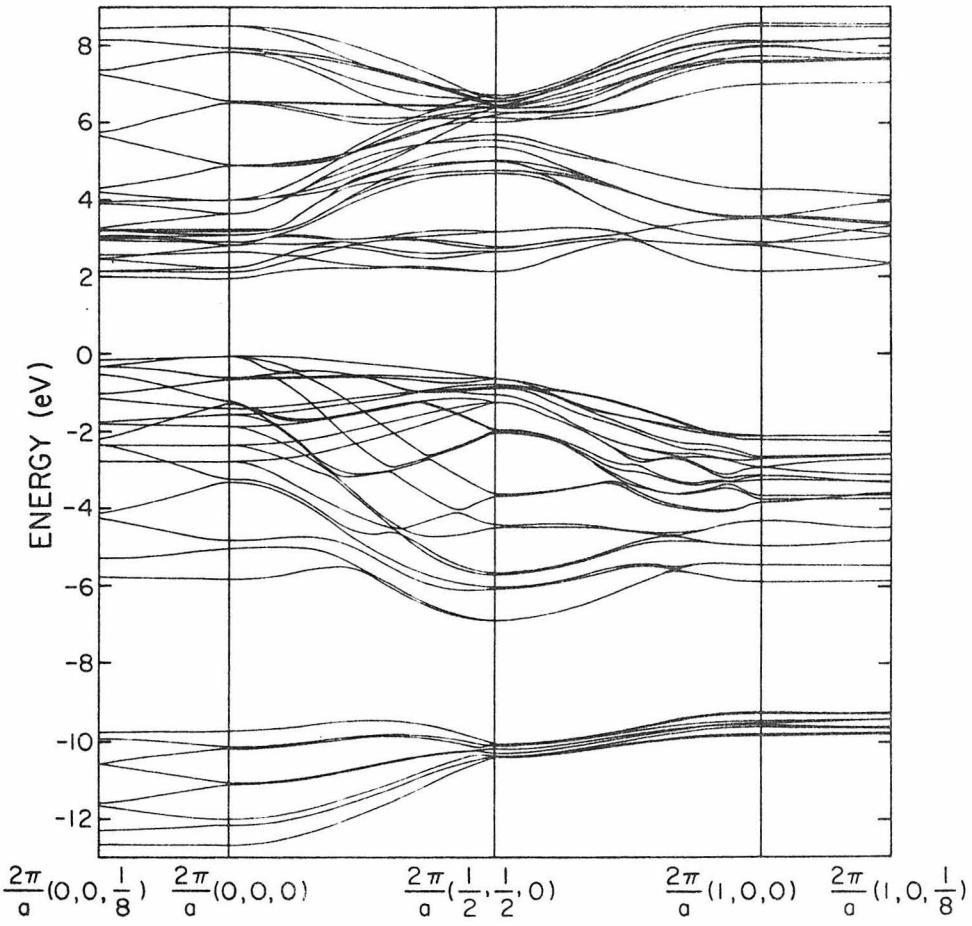
8
6
4
2
0
-2
-4
-6
-8
-10
-12
ENERGY (eV)
$\frac{2\pi}{a}(0,0,\frac{1}{8})$
$\frac{2\pi}{a}(0,0,0)$
$\frac{2\pi}{a}(\frac{1}{2},\frac{1}{2},0)$
$\frac{2\pi}{a}(1,0,0)$
$\frac{2\pi}{a}(1,0,\frac{1}{8})$

Figure 3.7

Figure 3.8

Valence band energies near the J-point (from the Γ-point) for the M=N=10 superlattice. Arrows indicate the interface states and the bands from which they are split off. VBE indicates the valence band edge.

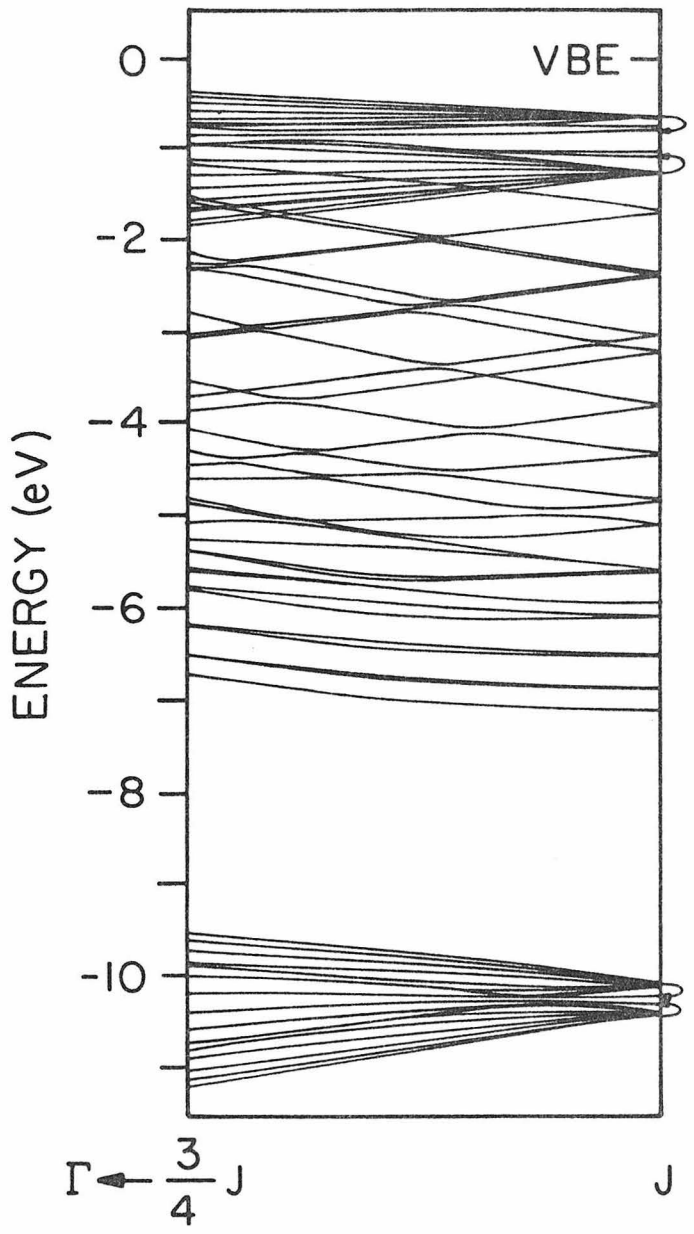

Figure 3.8

shown in Fig. 3.8 where the heads of arrows indicate the interface states and the tails of arrows indicate the grouping of bands from which these states are split off. All four interface states are located in energy gaps at the J-point. No interface states are found within the semiconducting band gap of the superlattice, however. The K-point has two or three states which have large squared amplitudes on the interface layers but which do not go to zero away from the interface. The Γ-point has no interface states.

The eigenvectors of the J-point whose energies are shown in Fig. 3.8 show that, except for the interface states indicated, the thick slabbed superlattice can also be described as a superposition of AlAs and GaAs bulk band structures as would be expected. Most states show pronounced AlAs or GaAs character. The energies of these states are very close to bulk values. The bulk energies corresponding to the J-point are found from the bulk 8 by 8 tight-binding matrix by diagonalizing that matrix for M+N values of the $\vec{k}$ vector as previously described. By combining the results of this procedure for both AlAs and GaAs, a comparison with the superlattice energies can be made. When the appropriate AlAs and GaAs bulk states are close in energy, a superlattice state occurs which has substantial amplitudes on both the AlAs and GaAs slabs, similar to the previously described K-point conduction band minimum state.

The four high concentrations of nine bands each from which the four interface states are split off are formed due to the small disper-

sion of the bulk bands in the z-direction away from the bulk L-point in both AlAs and GaAs. The dense sub-bands are formed when the bulk states with different k_z values are superimposed. The eigenvectors of these states reveal them to be almost identical in character to bulk states at the same energies. The interface states are the tenth member of these sub-bands. The two lowest sub-bands are related to the AlAs and GaAs bulk L_1^v states at -10.1 eV and -10.4 eV. The two interface states are split off by about .1 eV below the AlAs energy and .1 eV above the GaAs energy. The two sub-bands near the top of the valence band are almost identical in energy to the bulk L_3^v states at -.67 eV (AlAs) and -1.28 eV (GaAs). The GaAs interface state is split off by .2 eV and the AlAs interface state by about .15 eV.

VII. Densities of States

The transition of the electronic structure from interface to bulk was investigated using a density of states calculation. Fig. 3.9 shows the layer density of states for the M = N = 7 superlattice for the layers adjacent to the interface and for the layers located in the center of the AlAs and GaAs slabs. Also shown are the densities of states of bulk AlAs and bulk GaAs. The centers of the slabs, layers four and eleven, are seen to be similar to bulk AlAs and GaAs, respectively. Even the layers right adjacent to the interface, layers seven and fourteen, can be identified as being AlAs or GaAs-like, although they are not as bulk-like. Layers one more removed from the interface (not shown) substantially resemble the bulk. The interface state density is too small to make any noticeable contribution to the density of states in the form of separate peaks.

The charge density can be found by summing up the density of states over the valence band and is shown in Table IV. When this is done a charge density per layer much like the bulk results. If bulk AlAs or GaAs were to be divided up into layers like a superlattice, each layer would have exactly four of its eight tight-binding linear combinations filled with electrons (two per band) the same way on each layer. Because of the lack of translational symmetry perpendicular to the interface, there no longer must be the same charge on each layer. Table IV gives the corresponding numbers for the M=N=4 superlattice broken down to give the components on the anion and cation, and on the s and

Figure 3.9

Densities of states of bulk AlAs, bulk GaAs and layer densities of states for the M=N=7 superlattice. Densities of states are shown for layers adjacent to the interface and at the center of the AlAs and GaAs slabs. The bulk curves integrate to four, the number of states per atom (not including spin).

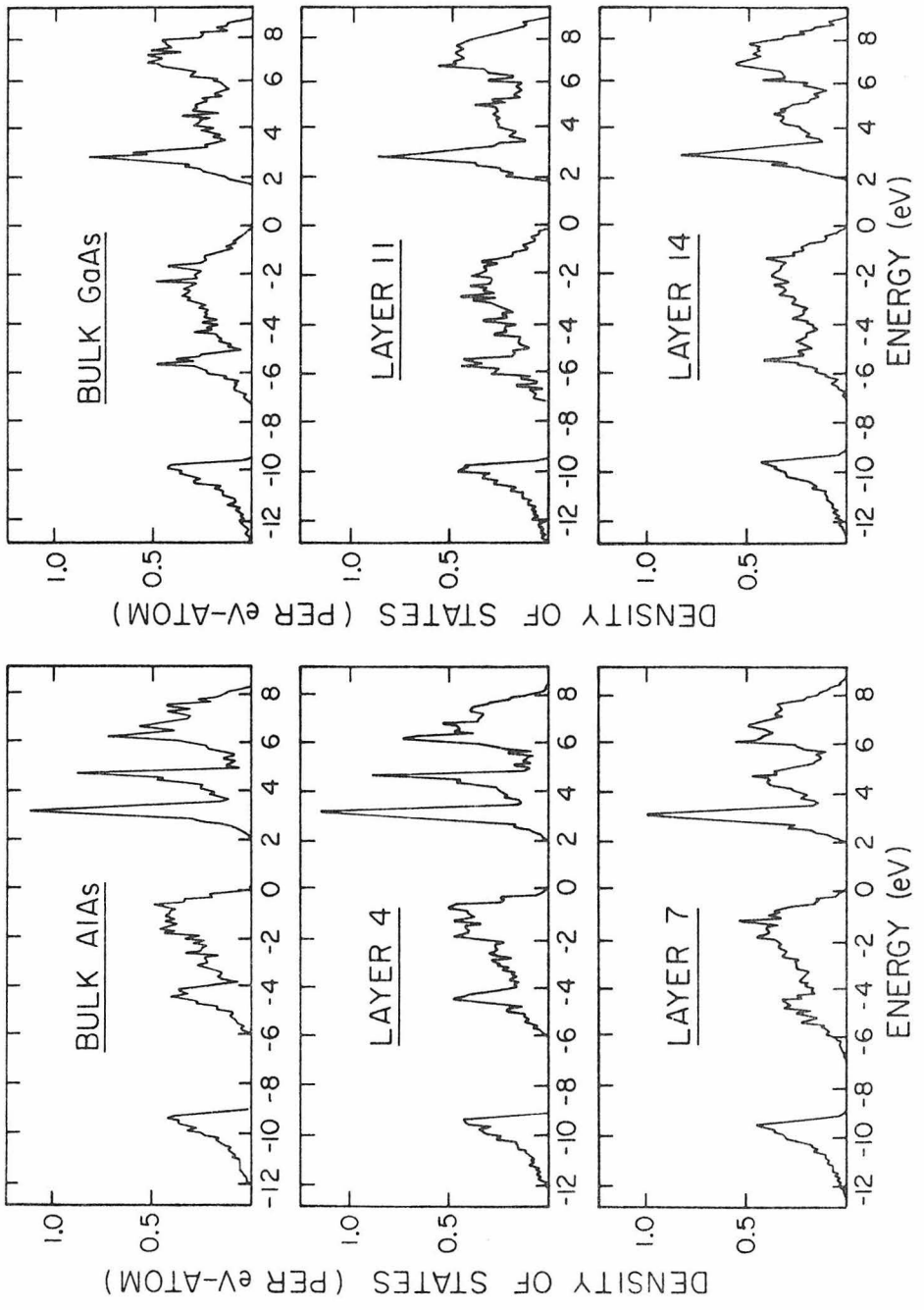
BULK AlAs
LAYER 4
LAYER 7
BULK GaAs
LAYER 11
LAYER 14
DENSITY OF STATES (PER eV-ATOM)
ENERGY (eV)
1.0
0.5
-12 -10 -8 -6 -4 -2 0 2 4 6 8

Figure 3.9

TABLE IV. Valence charge densities for bulk AlAs, bulk GaAs and the M=N=4 superlattice. The rows labelled s, p, and s+p contain the charge densities from the s-like states, the p-like states and the sums of these two respectively. The bulk charge densities each add up to eight, the number of valence electrons per unit cell. The sums of adjacent s+p values for the superlattice are also close to eight, except near the interface.

Bulk AlAs

	Al	As
s	1.08	1.47
p	2.77	2.68
s+p	3.85	4.15

Bulk GaAs

	Ga	As
s	1.12	1.53
p	2.43	2.92
s+p	3.55	4.45

M=N=4 Superlattice

	...	As	Al	As	Al	As	Ga	As	Ga	As	...
s		1.47	1.08	1.47	1.06	1.50	1.14	1.53	1.12	1.53	
p		2.68	2.77	2.67	2.71	2.80	2.49	2.92	2.44	2.92	
s+p		4.15	3.85	4.14	3.77	4.30	3.63	4.45	3.56	4.45	

↑

Interface Layer

p orbitals. These numbers differ from the bulk values only adjacent to the interfaces. The anion to cation ratio and the ratio of s-symmetry to p-symmetry squared amplitudes were also very close to bulk values. Most of the charge shift at the interface is due to a transfer of electrons from the Al to the Ga layers right next to the interface. The As interface layer has just the average charge of the two bulk As layers. Approximating this charge shift as being between two uniformly charged sheets parallel to the interface and located at the Al and Ga atoms results in an energy shift of just .21 eV.

VIII. Summary

The tight-binding method was used to investigate the electronic structure of the AlAs/GaAs superlattice and interface. Band gaps were determined as a function of AlAs and GaAs slab thicknesses and compared with those determined by optical experiments. The nature of the electronic states at the conduction band minimum and the valence band maximum were found. The results of other calculations concerning these states were discussed. Interface states were identified in the superlattice band structure as new energy levels appearing in valence band energy gaps. Finally, a layer density of states calculation was done to study the abruptness of the electronic character of the interface.

References to Chapter 3

1. L. Esaki and L. L. Chang, Crit. Rev. Solid State Sci. 6, 195 (1976).
2. R. Dingle, Crit. Rev. Solid State Sci. 5, 585 (1975).
3. A. G. Milnes and D. L. Feucht, Heterojunctions and Metal-Semiconductor Junctions (Academic Press, New York, 1972).
4. L. L. Chang and A. Koma, Appl. Phys. Lett. 29, 138 (1976).
5. R. Dingle, in Proceedings of the Thirteenth International Conference on the Physics of Semiconductors, Rome, 1976, edited by F. G. Fumi, (Tipografia Marves, Rome, 1977), p. 65.
6. J. L. Merz, A. S. Barker, Jr., and A. C. Gossard, Appl. Phys. Lett. 31, 117 (1977).
7. R. Dingle, W. Wiegmann, and C. H. Henry, Phys. Rev. Lett. 33, 827 (1974).
8. W. R. Frensley and H. Kroemer, Phys. Rev. B16, 2642 (1977).
9. D. Mukherji and B. R. Nag, Phys. Rev. B12, 4338 (1975).
10. E. Caruthers and P. J. Lin-Chung, Journal of Vacuum Science and Technology 15, 1459 (1978).
11. W. Andreoni, A. Baldereschi, and R. Car, Solid State Commun. 27, 821 (1978).
12. G. C. Osbourn and D. L. Smith, Phys. Rev. B19 (1979).
13. J. C. Slater and G. F. Koster, Phys. Rev. 94, 1498 (1954).
14. E. Hess, I. Topol, K. R. Schulze, H. Neumann, and K. Unger, Phys. Stat. Sol. (b) 55, 187 (1973).
15. J. R. Chelikowsky and M. L. Cohen, Phys. Rev. B14, 556 (1976).

16. D. J. Chadi, Phys. Rev. B16, 3572 (1977).

17. J. N. Schulman and T. C. McGill, Phys. Rev. Lett. 39, 1680 (1977).

18. B. Monemar, K. K. Shih, and G. D. Pettit, J. Appl. Phys. 47, 2604 (1976).

19. R. Tsu, A. Koma, and L. Esaki, J. Appl. Phys. 46, 842 (1975).

20. A. C. Gossard, P. M. Petroff, W. Wiegmann, R. Dingle, and A. Savage, Appl. Phys. Lett. 29, 323 (1976).

21. Impurities and defects could shift the emission peak away from the band gap value by several tens of millivolts.

Chapter 4

CdTe/HgTe SUPERLATTICE AND INTERFACE

I. Introduction

The study of superlattice systems made from alternating layers of two semiconductors has been a fruitful source of new knowledge about interfaces, band structures and novel quantum effects on a submicron scale. In this chapter we present the results of a theoretical study of the CdTe/HgTe superlattice, the third such system to be considered. The other two, AlAs/GaAs [1,2] and InAs/GaSb [3], have been sucessfully fabricated using the molecular beam expitaxy (MBE) technique. The CdTe/HgTe superlattice is also a likely candidate for fabrication using MBE because of their common zinc-blende form and close lattice match (within .3%)[4].

The distinctive features of this superlattice are the bulk band structures of the HgTe and CdTe, and the value of the offset between the valence band edges. CdTe is direct with a low temperature band gap of about 1.6 eV [4]. HgTe is a zero band gap semiconductor [4]. Its band structure is similar to CdTe except that relativistic effects have pulled down the Γ_6 symmetry s-like conduction band minimum of CdTe below the Γ_8 symmetry valence band maximum. The light hole valence band acquires a positive effective mass and is thus empty in the ground state. Empirical arguments, given in Section III of this paper, suggest that the offset between the valence band edges is small, if not zero. Hence, CdTe/HgTe superlattices consist of alternating layers of a large band gap semiconductor with a small band gap semiconductor.

We investigate several aspects of the electronic structure of the superlattice. Section II briefly discusses the tight-binding method and its application to the CdTe/HgTe superlattice. The problem of band edge discontinuities is dealtwith in Section III. Section IV describes the properties of the superlattice near the band gap edges including the value and nature of the band gap as a function of superlattice parameters. Section V discusses the confinement of the states at the conduction band minimum and valence band maximum and relates it to the bulk band structures. Section VI discusses the existence of interface states.

II. Calculation

The tight-binding method used in this calculation is similar to that used in Chapter 3. Hamiltonian matrix element parameters were determined for bulk CdTe and HgTe separately by reproducing the pseudopotential band structures of Katsuki and Kunimune [5]. The major difference in this calculation is that parameters representing terms due to the spin-orbit interaction are included. Cadmium, mercury, and tellurium all have more highly charged nuclear cores than aluminum, gallium, and arsenic. The electrons, therefore, are moving faster near the cores of the former atoms. Relativistic effects, including the spin-orbit interaction, become important [6]. The spin-orbit interaction has the form

$$H_{SO} = (\hbar/4m^2c^2) \left[\vec{\nabla}V \times \vec{p}\right] \cdot \vec{\sigma} \qquad (4.1)$$

where V is the total crystal potential and $\vec{\sigma}$ represents the Pauli spin matrices. This term couples different p-orbitals on the same atom only. Table I gives the form of H_{SO}. S-orbitals are not involved and are thus not shown. Each type of atom in the crystal has a term like this in the Hamiltonian. The spin-orbit parameter λ is different for each type. We used values of λ given in Reference 7. Relativistic terms other than the spin-orbit interaction are purely between an orbital and itself on a given atom and thus require no additional modification of the Hamiltonian matrix.

TABLE I. Form of the tight-binding Hamiltonian matrix with the addition of the spin-orbit interaction. Spin-orbit matrix elements with S-orbitals are zero and are not shown. The anion orbitals and the cation orbitals both have a matrix like this. H_o is the Hamiltonian matrix without spin-orbit.

$$
\begin{array}{c}
\\
x\uparrow \\
y\uparrow \\
z\uparrow \\
x\downarrow \\
y\downarrow \\
z\downarrow
\end{array}
\begin{array}{c}
\begin{array}{cccccc} x\uparrow & y\uparrow & z\uparrow & x\downarrow & y\downarrow & z\downarrow \end{array} \\
\begin{bmatrix}
0 & -i\lambda & 0 & 0 & 0 & \lambda \\
i\lambda & 0 & 0 & 0 & 0 & -i\lambda \\
0 & 0 & 0 & -\lambda & i\lambda & 0 \\
0 & 0 & -\lambda & 0 & i\lambda & 0 \\
0 & 0 & -i\lambda & -i\lambda & 0 & 0 \\
\lambda & i\lambda & 0 & 0 & 0 & 0
\end{bmatrix}
\end{array}
+
\begin{array}{c}
\\
\uparrow \\
\downarrow
\end{array}
\begin{array}{c}
\begin{array}{cc} \uparrow & \downarrow \end{array} \\
\begin{bmatrix} H_o & 0 \\ 0 & H_o \end{bmatrix}
\end{array}
$$

The parameters other than those due to the spin-orbit terms are listed in Table II. The resulting bulk band structures are shown in Fig. 4.1. Table III compares tight-binding and pseudopotential energy eigenvalues at some symmetry points in the Brillouin zone. In common with other tight-binding calculations, the valence bands closely resemble the pseudopotential bands. The conduction bands are somewhat flatter than in the pseudopotential case. We have not included d-states in our calculations. In both these compounds there are d derived bands which hybridize with and cross the bottommost valence bands [9] shown here. However, the precise character of these bottom valence bands are unimportant to our results, and hence for simplicity, we have excluded the d-bands.

TABLE II. Tight-binding parameters for CdTe and HgTe in the notation of Ref. 8. The subscripts 0 and 1 designate anion and cation, respectively.

		CdTe	HgTe
1.	$E_{ss}(000)_0$	-6.157 eV	-8.357 eV
2.	$E_{ss}(000)_1$	- .519	.915
3.	$E_{xx}(000)_0$	2.871	1.856
4.	$E_{xx}(000)_1$	2.590	.738
5.	$E_{ss}(\frac{1}{2}\frac{1}{2}\frac{1}{2})$	-1.182	-1.151
6.	$E_{sx}(\frac{1}{2}\frac{1}{2}\frac{1}{2})_{01}$	1.422	1.382
7.	$E_{sx}(\frac{1}{2}\frac{1}{2}\frac{1}{2})_{10}$	.930	.799
8.	$E_{xx}(\frac{1}{2}\frac{1}{2}\frac{1}{2})$	.808	.597
9.	$E_{xy}(\frac{1}{2}\frac{1}{2}\frac{1}{2})$	1.227	1.085
10.	$E_{xy}(110)_0$	.062	.040
11.	$E_{xy}(110)_1$	.123	.567
12.	$E_{xx}(110)_0$	.080	.321
13.	$E_{xx}(110)_1$	.167	.185
14.	$E_{xx}(011)_0$	- .140	- .376
15.	$E_{xx}(011)_1$	- .226	- .199
16.	$E_{sx}(110)_0$	.028	.216
17.	$E_{ss}(110)_0$	.001	.068
18.	$E_{ss}(110)_0$	- .227	- .377
19.	$E_{ss}(110)_1$	- .008	- .238

Figure 4.1

Bulk band structures calculated by the tight-binding method for CdTe and HgTe. The valence band maximum is set to 0 eV.

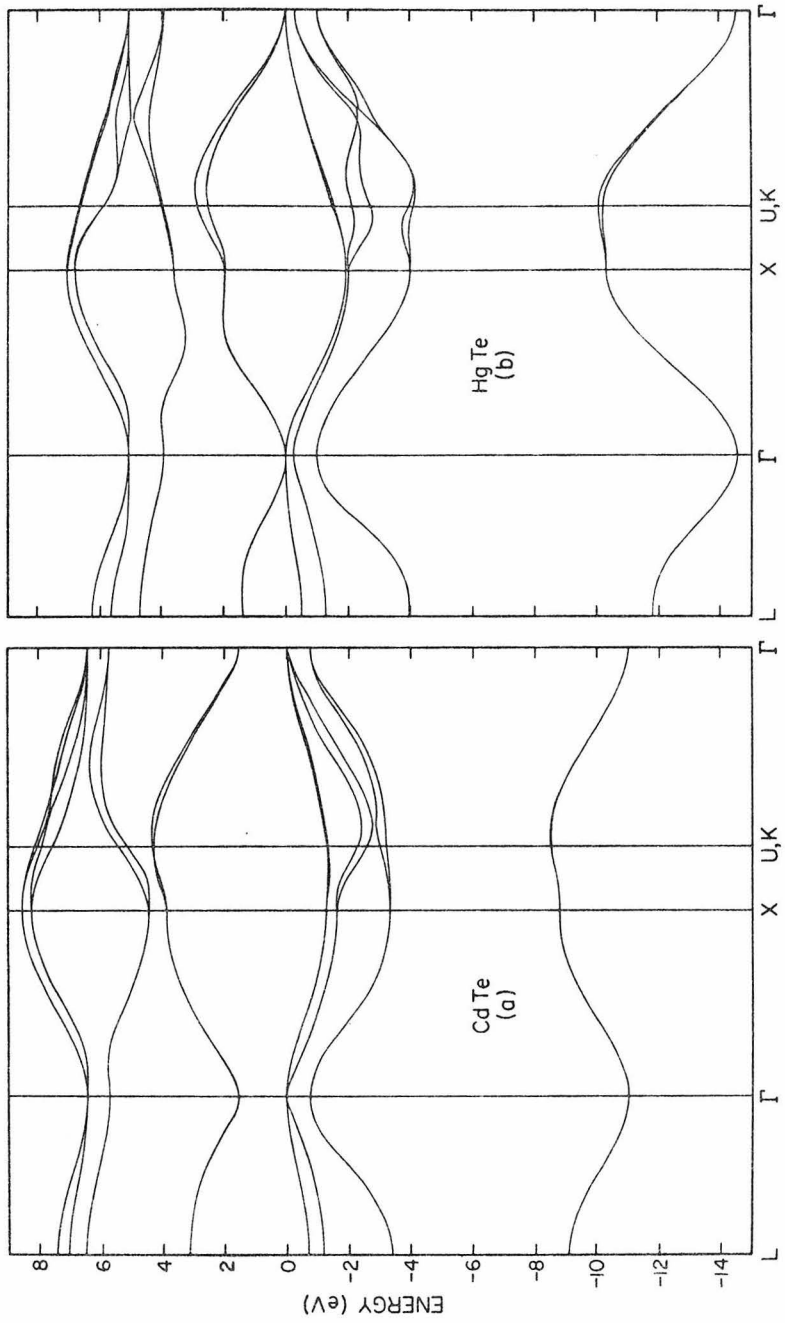

Figure 4.1

TABLE III. CdTe and HgTe Bulk Energy Levels Calculated Using Tight-binding and Pseudopotential Methods

Level	CdTe		HgTe	
	Tight-binding	Pseudopotential (5)	Tight-binding	Pseudopotential (5)
Γ_{7V}	- .76 eV	- .728 eV	-1.00 eV	- .893 eV
Γ_{8V}	0	0	0	0
Γ_{6C}	1.53	1.591	- .26	- .280
Γ_{7C}	5.74	6.171	3.93	4.179
Γ_{8C}	6.47	6.461	5.04	5.040
L_{6V}	-3.4	-3.3	-4.0	-4.1
L_{6V}	-1.21	-1.008	-1.30	-1.298
L_{4V}	- .72	- .546	- .53	- .672
L_{6C}	3.16	3.091	1.37	1.252
L_{6C}	6.52	6.606	4.70	4.866
L_{4C}	7.07	6.695	5.64	5.194
X_{7V}	-3.3	-3.3	-4.04	-4.0
X_{7V}	-1.61	-1.658	-1.95	-2.056
X_{6V}	-1.28	-1.320	-2.02	-1.826
X_{6C}	3.89	3.900	1.95	1.830
X_{7C}	4.46	4.410	3.61	2.705
K_{3V}	-3.2	-3.2	-4.1	-3.7
K_{3V}	-2.59	-2.409	-2.71	-2.884
K_{3C}	-1.32	-1.258	-1.51	-1.646
K_{3C}	4.29	4.173	2.51	2.283
K_{3C}	5.16	5.527	3.97	4.170

III. Band Discontinuities

One additional parameter must be determined before the bulk parameters can be incorporated in the superlattice Hamiltonian matrix, the value of the valence band edge discontinuity between the two materials. It is this offset parameter which establishes the way in which the bands line up when the heterojunction is formed. Its effect on the band structure of superlattices has been explored for the two previous cases, AlAs/GaAs [10] and InAs/GaSb [11]. Its effect in the CdTe/HgTe case will be discussed in Sections IV and V.

The band discontinuities used for the AlAs/GaAs superlattice were derived from experimental results, as explained in Chapter 3. There are no experimental data available in this case, as the CdTe/HgTe superlattice has not yet been fabricated. At the present time there has also been no first principles theory applied to this problem. In this section we give empirical arguments which allow us to choose a value for the discontinuity.

We have chosen this parameter to be zero for the following reasons. One model of heterojunction band line-ups uses the electron affinities of the two materials to locate the conduction band edges [12]. It is assumed in this model that putting the materials into a heterojunction does not change the relative conduction band positions at the interface. The valence band discontinuity, ΔE_V, is then just the difference between the electron affinity plus band gap (ionization potential, Φ) of the two.

$$\Delta E_V = \Phi_{CdTe} - \Phi_{HgTe}$$

The HgTe ionization potential has been measured by N. J. Shevchik, et al.[9] to be 5.9 eV. Both Shevchik [9] and R. K. Swank [13] have measured this quantity for CdTe and report 6.2 eV and 5.8 eV, respectively. These values of Φ yield values of ΔE_V of 0.3 and -0.1 eV, respectively. Further evidence that the discontinuity is small is given in Fig. 4.2. The band gap plus electron affinity of several III-V and II-VI compounds are shown there. The values are from Sharma and Purohit [14] (including Swank's CdTe value), except for the HgTe number which is from Shevchik [9]. It can be seen that the ionization potential is more heavily dependent on the anion than the cation [15], and that differences between compounds with the same anion (especially for the tellurium case) are small. We use a value of zero for the discontinuity, although a small value similar to that for the AlAs/GaAs heterojunction would not be unexpected. This implies that the conduction band discontinuity is equal to the difference in the band gaps of CdTe and HgTe, as shown in Fig. 4.3.

Figure 4.2

Band gap plus electron affinity for several III-V and II-VI compounds. This is an approximation to the energy difference between the vacuum and the top of the valence band. The HgTe value is from reference 9. All others are from reference 14.

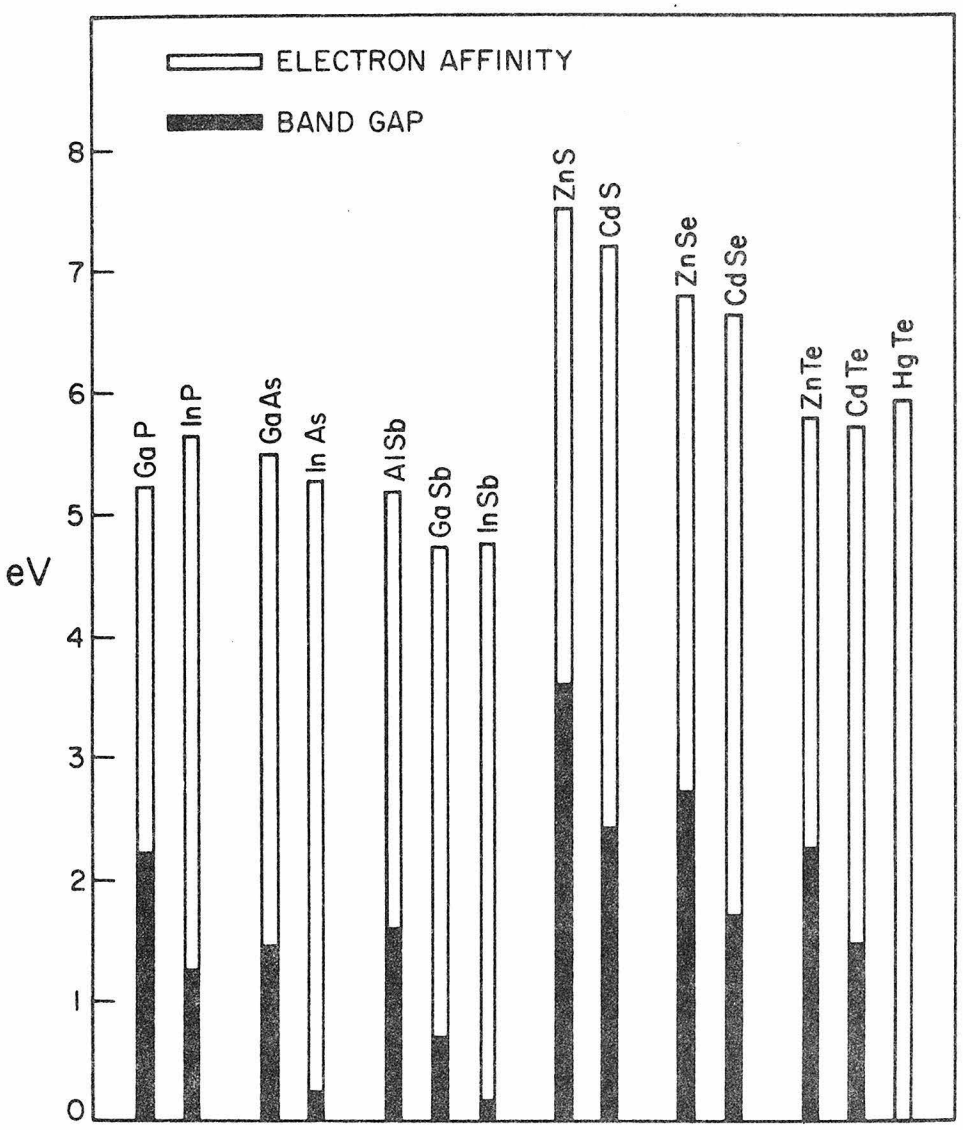
ELECTRON AFFINITY
BAND GAP
eV
0
1
2
3
4
5
6
7
8
Ga P
In P
Ga As
In As
Al Sb
Ga Sb
In Sb
Zn S
Cd S
Zn Se
Cd Se
Zn Te
Cd Te
Hg Te

Figure 4.2

Figure 4.3

Energy band discontinuities for the CdTe/HgTe superlattice. The valence band discontinuity is zero. The conduction band discontinuity equals the band gap difference, 1.6 eV.

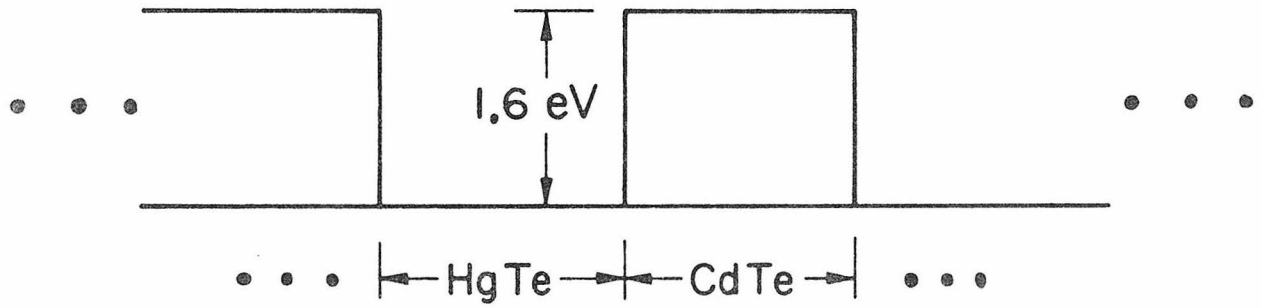

Figure 4.3

IV. Band Gap Properties

The band gap of the CdTe/HgTe superlattice differs from that of the random $Hg_{1-x}Cd_xTe$ alloy in two ways. First, the value of the gap for a fixed cadmium to mercury ratio varies as a function of the CdTe and HgTe repeated slab thicknesses. Second, the symmetry of the state at the valence band maximum exhibits a crossover between two symmetry types as the thickness is varied. This section discusses these features of the band gap.

Figure 4.4 shows the variation in the band gap versus HgTe layer thickness for superlattices with three ratios of CdTe layer thickness to total repeated slab thickness (x). The three horizontal line segments indicate the random $Hg_{1-x}Cd_xTe$ alloy band gaps calculated with our tight binding parameters in the virtual crystal approximation with the same values of x. It can be seen that for thin layers the band gap differs only slightly from the random alloy value. As the HgTe layer thickness increases, the gap decreases monotonically and approaches the bulk HgTe zero band gap limit. In common with the alloy, higher cadmium concentrations produce larger band gaps.

This band gap variation can be understood intuitively using a simple model. The zero band gap HgTe is envisioned as forming wells for the conduction electrons with the CdTe/HgTe conduction band discontinuity forming the sides of the wells (Fig. 4.3). As the HgTe

Figure 4.4

Superlattice band gaps versus number of atomic layers of HgTe in a repeated superlattice slab. The dashed line represents superlattices with a CdTe to HgTe ratio of 2:1; the solid line, 1:1; and the dotted line, 1:2 (x=2/3, 1/2, and 1/3). The random alloy values are indicated by the three long horizontal dashes.

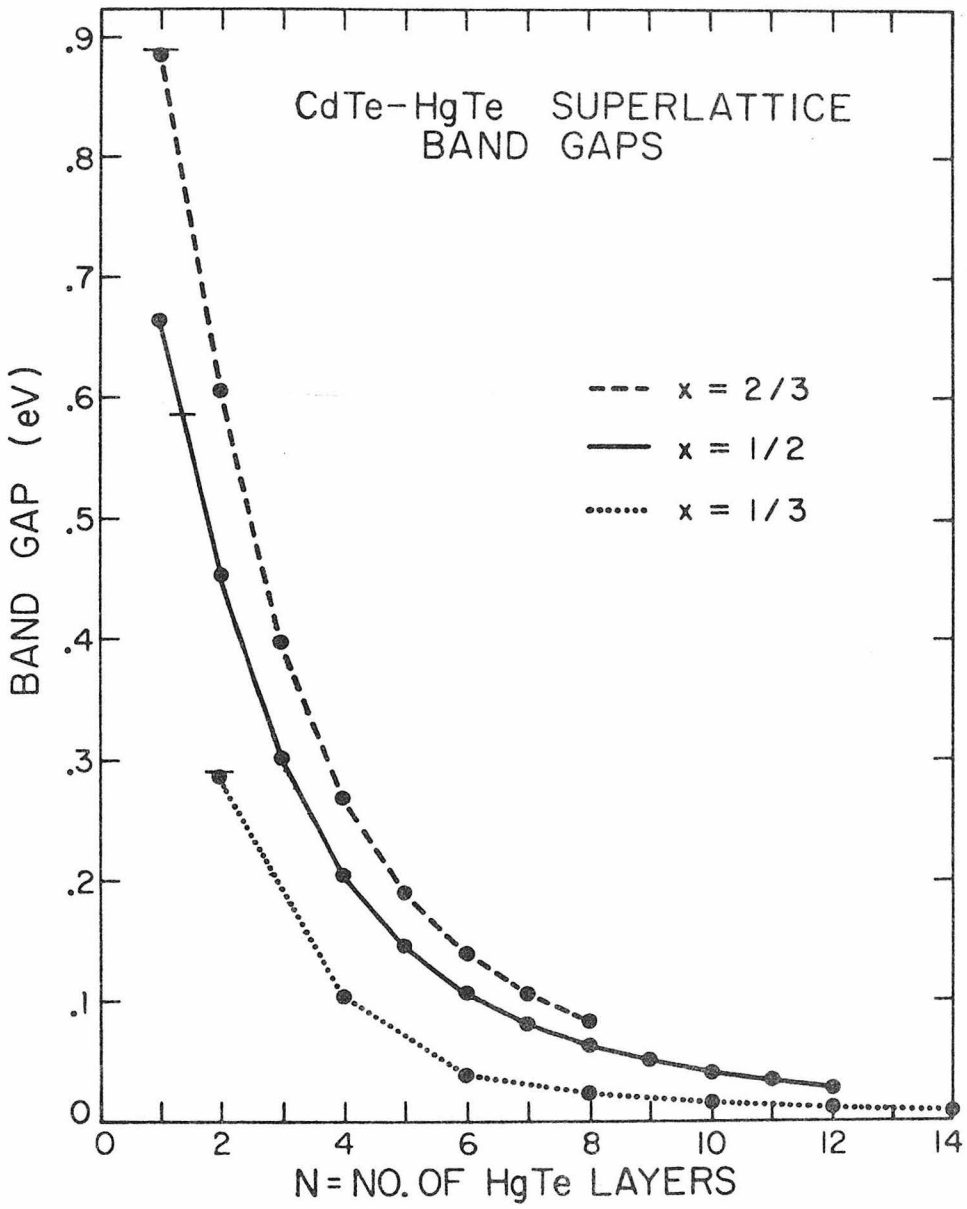
CdTe-HgTe SUPERLATTICE
BAND GAPS
x = 2/3
x = 1/2
x = 1/3
BAND GAP (eV)
N = NO. OF HgTe LAYERS
0
.1
.2
.3
.4
.5
.6
.7
.8
.9
0
2
4
6
8
10
12
14

Figure 4.4

well width is increased, the energy of the lowest well state decreases and thus the band gap decreases. Because of the zero valence band discontinuity, the hole states are not confined in either the CdTe or HgTe layers in this way.

The switch in symmetry of the valence band maximum state as the thicknesses are varied will now be discussed. CdTe and HgTe have a different ordering of states at $\vec{k} = 0$. The Γ_6 symmetry conduction band minimum state goes below the Γ_8 symmetry valence band maximum state as the mercury concentration is increased for the $Hg_{1-x}Cd_xTe$ alloy (Fig. 4.5). An interesting feature of the superlattice system is that this same behavior can occur with the superlattice for a <u>given</u> cadmium concentration as slab thickness is varied. This is demonstrated in Fig. 4.6. It shows the change in energy levels for states near the band gap as a function of layer thickness. Panels (a), (b), and (c) are for superlattices with three ratios of CdTe to HgTe layer thickness. In Fig. 4.6(a) the HgTe layers are twice as thick as the CdTe layers; in Fig. 4.6(b) the layers are of equal thickness, and in Fig. 4.6(c) the CdTe layers are twice as thick as the HgTe layers. The three curves in each panel represent the energies at the bottom of the conduction band, the top of the valence band, and the next state in energy below the top of the valence band. All states have k-vectors at the center of the Brillouin zone. The horizontal axis gives the number of atomic layers of HgTe per repeated superlattice slab.

Figure 4.5

Details of the band structure of the $Hg_{1-x}Cd_xTe$ random alloy for values of x such that (a) the Γ_6 state lies above the Γ_8 state and (b) the Γ_6 state lies below the Γ_8 state. Δ is the Γ_7-Γ_8 spin-orbit splitting. The Γ_8 state is at the top of the valence band in both cases. This picture is schematic only.

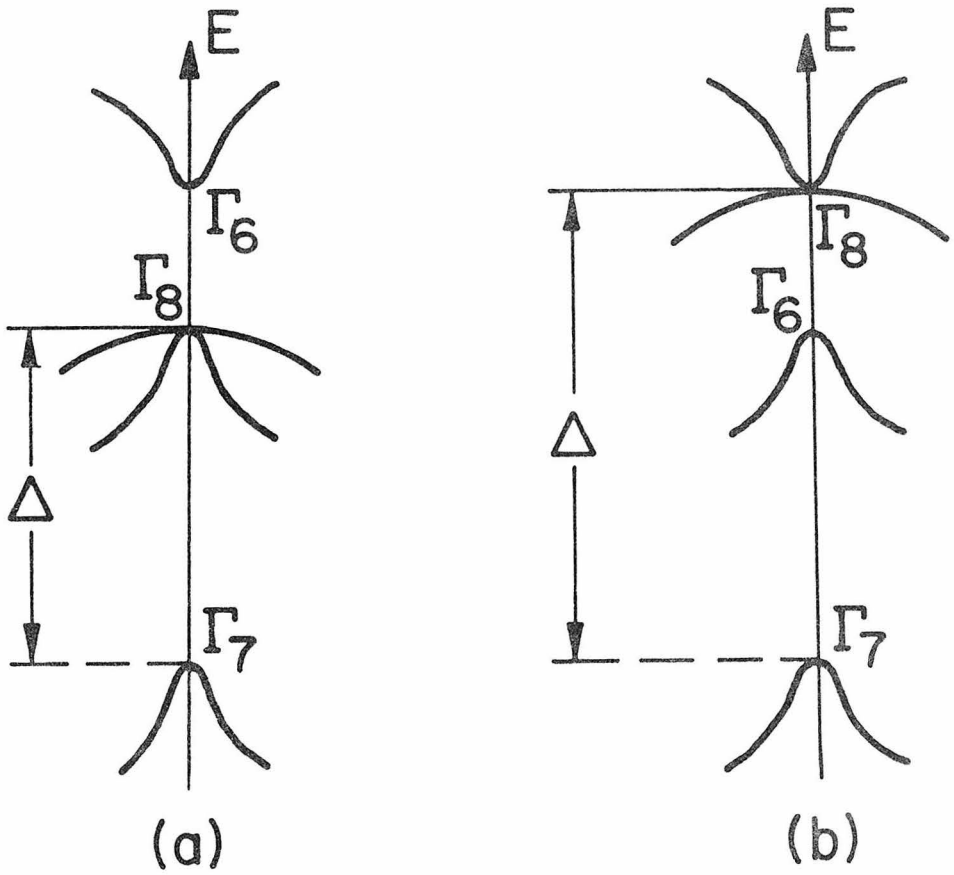

Figure 4.5

Figure 4.6

Three superlattice energies at the band gap edges. The band gap is between the two higher energy states. Γ_6^S states are indicated by open triangles, and Γ_7^S states by filled circles. M and N are the number of CdTe and HgTe atomic layers per slab.

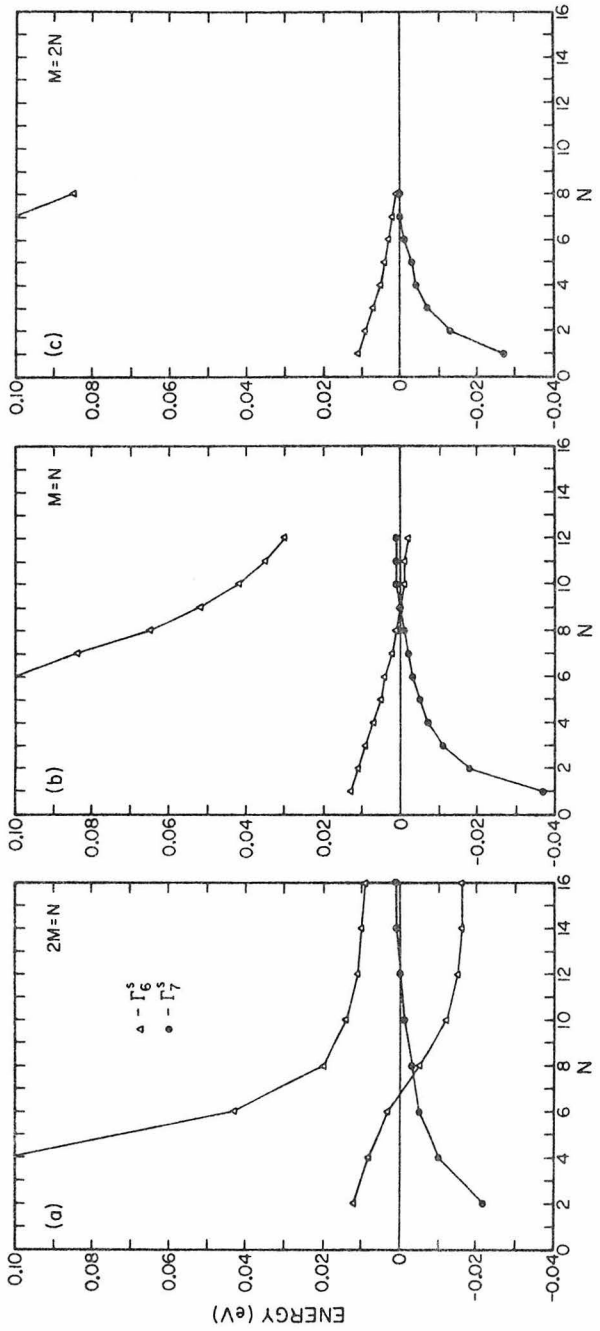
2M=N
M=N
M=2N
(a)
(b)
(c)
Δ - Γ_6^s
• - Γ_7^s
ENERGY (eV)
N
0.10
0.08
0.06
0.04
0.02
0
-0.02
-0.04
0
2
4
6
8
10
12
14
16

Figure 4.6

The crossing of the curves in panels (a) and (b) (and thus the change in symmetry of the valence band maximum) can be interpreted in terms of the bulk zincblende states from which they are derived, but first the relationship between the bulk and superlattice state symmetries must be described. The three bulk zincblende symmetries Γ_6^B, Γ_7^B, and Γ_8^B are modified when the periodic perturbation in the z direction is superimposed. (The superscript B indicates the irreducible representation of the bulk point group T_d.) Only two group representations, which we call Γ_6^S and Γ_7^S, are possible. (The superscript S indicates the irreducible representation of the superlattice point group D_{2d}.) The Γ_6^B conduction band state becomes a state with Γ_6^S symmetry in the superlattice case. The split off Γ_7^B valence band state becomes a Γ_7^S symmetry state. The four-fold degenerate Γ_8 state at the valence band maximum splits into two spin doubly degenerate superlattice states, one of Γ_6^S symmetry and one of Γ_7^S symmetry [16].

The different order of these states in energy as a function of layer thickness produces the crossover. Intuitively what might be expected to happen is that for thin alternating layers the ordering of the states would be similar to that for the random alloy with the same cadmium concentration. All three cadmium concentrations dealt with in Fig. 4.6 produce random alloy band structures with the Γ_6^B energy higher than Γ_8^B. The Γ_6^B, Γ_8^B ordering should switch for layers thick enough to reconstitute bulk HgTe. This is what is shown in Fig. 4.6 if the top-lying Γ_6^S state is interpreted in terms of bulk states correctly. It

is derived from bulk Γ_6^B or Γ_8^B. For thin layers it is derived from the conduction band minimum Γ_6^B state. Its energy relative to the valence band maximum is close to that for the $Hg_{1-x}Cd_xTe$ random alloy of the same cadmium to mercury ratio as shown in Fig. 4.4. For thick layers it becomes the higher energy state of the pair of states which the bulk Γ_8^B level splits into. The higher energy Γ_6^S state does not actually pass through the other states. Only the lower energy Γ_6^S state crosses the Γ_7^S state as shown in (a) and (b). The HgTe layers in Fig. 4.6(c) are not thick enough to exhibit the crossing. The degree to which the HgTe layers are approaching bulk HgTe is measured by the energy difference between the higher energy Γ_6^S state and the Γ_7^S state. The thickest layer consists of sixteen atomic HgTe layers alternating with eight of CdTe shown in Fig. 4.6(a). The states are still about 10 meV apart at this thickness.

V. Confinement of States

This section discusses the effects of the bulk band structures and the relative positioning of these band structures on the confinement of the superlattice electronic states at the valence band maximum and the conduction band minimum. The confinement of the states in the CdTe/HgTe superlattice is compared with that previously discussed in Chapter 3 for the AlAs/GaAs superlattice. The zero valence band maximum discontinuity and the zero band gap of HgTe result in substantially less confinement in the CdTe/HgTe case.

The valence band maximum state will be discussed first. Figure 4.7 shows the wave functions of two superlattice states for the CdTe/HgTe superlattice consisting of ten layers of CdTe alternating with ten layers of HgTe. These states are located in energy at the top of the valence band and the bottom of the conduction band. Both band extrema states are located in $\vec{k}$ space at the center of the Brillouin zone ($\vec{k}$=0). The figure shows the anion (Te) and the cation (Cd and Hg) charge distributions per atomic layer for each state. The first ten layers are CdTe and the second ten are HgTe. The valence band state shown in this figure is to be compared with the state shown in Fig. 3.6(c). That is the valence maximum state for the AlAs/GaAs ten on ten superlattice.

The zero valence band discontinuity results in the CdTe/HgTe state being almost uniform across the slab. In contrast, the AlAs/GaAs

Figure 4.7

Conduction (bottom) and valence (top) band edge state anion (Te) and cation (Cd and Hg) charge distributions for a superlattice consisting of ten layers of CdTe alternating with ten layers of HgTe. The dotted line is for the anion and the solid line for the cation.

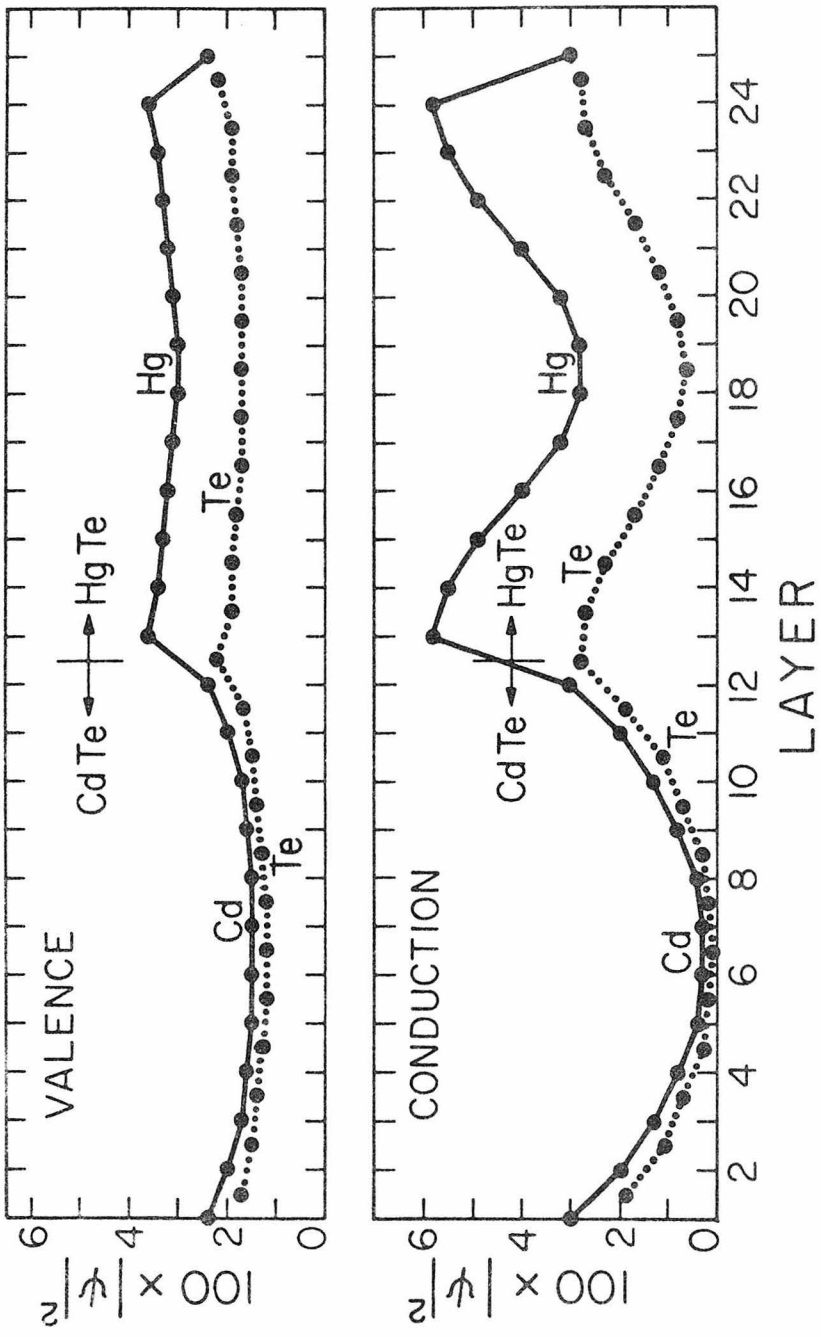
VALENCE
CONDUCTION
CdTe
HgTe
Hg
Te
Cd
Te
100 × |ψ|²
0
2
4
6
2
4
6
8
10
12
14
16
18
20
22
24
LAYER

Figure 4.7

state has a pronounced peaked structure in the GaAs layers characteristic of well-like behavior. This is caused by the approximately .2 eV AlAs/GaAs valence band maximum discontinuity, as discussed in Chapter 3.

The degree of confinement of the conduction band minimum state is shown in Fig. 4.7. The AlAs/GaAs superlattice conduction band minimum state shown in Fig. 3.6(d) dies off more quickly in the AlAs slab than the corresponding CdTe/HgTe superlattice state does in the CdTe slab. To understand this, it is necessary to examine these states in more detail.

A superlattice state can be regarded as being made up from bulk CdTe and bulk HgTe states which are matched at the interfaces. The bulk states must have the same value of the wave vector parallel to the interface ($\vec{k}_{||}$). The energy of the superlattice conduction band minimum state lies 0.04 eV above the CdTe valence band maximum and thus the appropriate CdTe bulk states must have complex values of k_z, the wave vector perpendicular to the interfaces. [17] To estimate how rapidly the state should decay into the CdTe we need the value of the imaginary part of $k_z(k_{zi})$. For values of the energy near the valence band edge in CdTe we can estimate the smallest values of k_{zi} from the expression

$$k_{zi} = \sqrt{\frac{2m^*}{\hbar^2} |\Delta E|} \qquad (4.1)$$

where ΔE is the energy difference between the state in question and the valence band edge and m* is the effective mass. This is just the effective mass approximation for complex $\vec{k}$. Our tight-binding calculation for CdTe yields effective masses of 0.82 m_e and .21 m_e for the two Γ_8 derived bands (see Fig. 4.5) and .46 m_e for the Γ_7 derived band. With ΔE=.04 eV, the number of layers necessary for a decrease in probability of e is 1.6, 3.2, and 0.4, respectively for these three masses. These decay lengths are in agreement with the slow decay of the wave function found by closer examination of this state.

This explanation also indicates the sensitivity of the state confinement to the valence band off-set. Changing the valence band discontinuity in such a way as to increase ΔE would decrease the decay length, as indicated by Eq. (4.1).

The transport properties of the superlattice perpendicular to the interfaces are governed by the degree of localization of the band edge states. The dispersion in these bands is influenced by the degree of confinement of the states in the HgTe slabs. A lesser degree of confinement results in a smaller effective mass perpendicular to the interfaces, and thus greater mobility in that direction. The relative delocalization of the CdTe/HgTe states has implications concerning the usefulness of this superlattice material in opto-electronic devices.

VI. Interface Properties

In the limit in which the superlattice layers are made large, the series of interfaces become isolated from each other. The thickest superlattices investigated by us have a total of twelve CdTe and HgTe layers each per repeated slab. As indicated in the previous section the single heterojunction limit has not yet been reached at this thickness. A comprehensive search for interface states cannot be accomplished for this reason. Interface states which die off very abruptly within two or three atomic layers from the interface can, however, be identified. Two states of this type have been found at the CdTe/HgTe interface near and at the Brillouin zone boundary. One has an energy approximately 2.6 eV below the valence band maximum. It has significant amplitude on about six layers surrounding the interface. The other interface state is at an energy which may make it more accessible to experimental methods. Its energy is 0.45 eV below the valence band maximum, but it is the topmost state at that particular point on the Brillouin zone boundary, the J-point. Away from this point the state acquires a bulk-like character. There are no interface states at the center of the Brillouin zone. Results concerning interface states are more sensitive to the particular tight-binding parameters used than band structure results.

VII. Summary

The tight-binding method was used to calculate the electronic structure of the CdTe/HgTe superlattice and interface. The band gaps were found to decrease monotonically with increasing HgTe slab thickness. For thin slabbed superlattices, the gaps are close to those of the random alloy with the same composition. The symmetry of the valence band maximum state was found to change at certain HgTe slab thicknesses. This is explained by relating the superlattice states to bulk CdTe and HgTe states. The confinement of the states at the band edges was examined and less localization was found than for the AlAs/GaAs superlattice. Finally, interface states were investigated and found near the boundary of the Brillouin zone.

References to Chapter 4

1. L. L. Chang, L. Esaki, W. Howard, R. Ludeke, and G. Schul, J. Vac. Sci. Technol. 10, 655 (1973).
2. R. Dingle, A. C. Gossard, and W. Wiegmann, Phys. Rev. Lett. 34, 1327 (1975).
3. H. Sakaki, L. L. Chang, G. A. Sai-Halasz, C. A. Chang, and L. Esaki, Solid State Commun. 26, 589 (1978).
4. R. Dornhaus and G. Nimtz, Springer Tracts in Modern Physics 78 (1976).
5. S. Katsuki and M. Kunimune, J. Phys. Soc. Japan 31, 415 (1971).
6. A. Kisiel and P. M. Lee, J. Phys. F 2, 395 (1972).
7. F. Herman, C. D. Kuglin, K. F. Cuff, R. L. Kortum, Phys. Rev. Lett. 11, 541 (1963).
8. J. C. Slater and G. F. Koster, Phys. Rev. 94, 1498 (1954).
9. N. J. Shevchik, J. Tejeda, M. Cardona, and D. W. Langer, Phys. Stat. Sol. (b) 59, 87 (1973).
10. R. Dingle, W. Wiegmann, and C. H. Henry, Phys. Rev. Lett. 33, 827 (1974).
11. G. A. Sai-Halasz, R. Tsu, and L. Esaki, Appl. Phys. Lett. 30, 651 (1977).
12. A. G. Milnes and D. L. Feucht, Heterojunctions and Metal-Semiconductor Junctions (Academic Press, New York, 1972) pp 3-13.

13. R. K. Swank, Phys. Rev. 153, 844 (1967).

14. B. L. Sharma and R. K. Purohit, Semiconductor Heterojunctions (Pergamon Press, Oxford, 1974).

15. J. O. McCaldin, T. C. McGill, and C. A. Mead, J. Vac. Sci. Technol. 13, 802 (1976).

16. G. F. Koster, J. O. Dimmock, R. G. Wheeler, H. Statz, Properties of the Thirty-two Point Groups (The Massachusetts Institute of Technology Press, Cambridge, Mass., 1963).

17. See for example V. Heine, Proc. Phys. Soc. 81, 300 (1963) for a discussion of some of the general features of complex band structures.